A Numerical Study of Fuel Stratification, Heat Transfer Loss, Combustion, and Emissions Characteristics of a Heavy- Duty RCCI Engine Fueled by E85/Diesel

A Numerical Study of Fuel Stratification, Heat Transfer Loss, Combustion, and Emissions Characteristics of a Heavy-Duty RCCI Engine Fueled by E85/Diesel

A. Willems[1], P. Rahnama[1,2], B. Somers[1] and R. Novella[2]

[1] Power & Flow – Department of Mechanical Engineering. Technical University of Eindhoven. P.O. Box 513, 5600 MB Eindhoven, The Netherlands.

[2]CMT – Motores Térmicos. Universidad Politécnica de Valencia. Camino de Vera s/n, E-46022 Valencia, Spain.

E-mail: pouryarahnama@gmail.com

Abstract. Reactivity-controlled compression ignition is a new advanced combustion strategy developed to reach cleaner and more efficient combustion by controlling fuel stratification inside the engine cylinder and reducing heat loss. While its potential to produce high efficiency and low emissions and to reach higher loads than other Low-Temperature Combustion strategies (LTC) has been confirmed numerous times, its operating range is still limited to moderate loads. One potential solution to increase the operating range is using E85 fuel as the premixed fuel due to the potential of providing a longer combustion duration. This work will focus on developing a computational fluid dynamics (CFD) model for a reactivity-controlled compression ignition (RCCI) engine fueled by E85/diesel with a double step piston bowl geometry. The model is used to investigate the effects of four different design parameters, namely injection timing, boost pressure, initial temperature, and spray included angle, to identify their impact on all crucial parameters describing combustion i.e. the stratification level, heat loss, and emissions characteristics. It has been found that the start of injection affects the fuel stratification levels inside the cylinder, with the optimum location for efficiency located in the moderate stratified region. The boost pressure mainly influences the mean gas temperature, the start of combustion, combustion duration, and the recession time of the Heat Release Rate (HRR) curve. It is found that the boost pressure does not have an influence on the heat loss of the engine and the heat loss is more correlated to flame temperature than the average temperature. It is also proven that the boost pressure could assist in the suppression of NOx, but when the intake pressure is too high, the thermal efficiency drops. Furthermore, the results show that the initial temperature is preferred to be as low as possible but sufficiently high enough to burn all the introduced fuel. Intake temperature alters the HRR shape and combustion duration significantly. Lastly, it is found that the combination of the spray included angle and piston bowl geometry can substantially determine the way the flame is formed and its location. The study on the effect of spray angle provides essential insights on the origin of unburned hydrocarbon emission, HRR shape, and heat loss.

Notation

AMR *Adaptive mesh refinement*
ATDC *After top dead centre*
BDC *Bottom dead center*
CA50 *Crank angle of 50% cumulative heat release*
CAD *Crank angle degree*
BDC *Bottom dead center*
CDC *Conventional diesel combustion*
CFD *Computational fluid dynamics*
CO_2 *Carbon dioxide*
CO *Carbon monoxide*
DI *Direct Injection*
DTBP *Di-tert-butyl peroxide*
E85 *Fuel blend of 85% ethanol to 15% gasoline volume-based*
EGR *Exhaust gas recirculation*
EVO *Exhaust valve opening*
GHG *Greenhouse gas*
HCCI *Homogeneous charge compression ignition*
HC *Hydrocarbons*
HECC *High-efficiency clean combustion*
HRF *High reactivity fuel*
HRR *Heat release rate*
IC *Internal combustion*
IDT *Ignition delay time*
IT *Initial temperature*
IVC *Intake valve closure*
LFS *Laminar flame speed*
LHV *Lower heating value*
LRF *Low reactivity fuel*
LTC *Low-temperature combustion*
NOx *Oxides of nitrogen*
NTC *No time counter*
PFI *Port fuel injection*
PPCI *Partially premixed compression ignition*
PPLTC *Partially premixed low-temperature combustion*
PRF *Primary reference fuel*
RANS *Reynolds-Averaged Navier-Stokes*
RCCI *Reactivity controlled compression ignition*
RNG *Renormalization group*
SCCI *Stratified charge compression ignition*
SOC *Start of combustion*
SOI *Start of injection*
TDC *Top dead center*

1. Introduction

Internal combustion (IC) engines are heavily integrated into society with their primary purpose to produce mechanical power from the chemical energy contained in fuel by a chemical process called combustion, which burns or oxidizes the fuel inside the enclosed space of the engine [1]. The most common fuels used in this process are gasoline and diesel, also known as fossil fuels. IC engines operating on fossil fuels [2] produce about 10% of the world's greenhouse gas (GHG) emissions [3] and produce hazardous exhaust emissions such as carbon monoxide (CO), oxides of nitrogen (NOx) and soot. Concerns and regulations about the emission of GHG and dangerous exhaust emissions have guided research into internal combustion engines further towards cleaner and more efficient combustion to reduce these emissions [4, 5]. The application of alcoholic fuels in IC engines is under spotlight due to their high enthalpy of vaporization, octane number, flame speed, and low adiabatic flame temperature.

As a result, new advanced combustion strategies with renewable fuels are being developed, and most of these strategies can be categorized under low-temperature combustion (LTC) [6]. An LTC mode engine works at lower combustion temperatures compared to conventional diesel mode engines [7]. The benefit of having a lower combustion temperature is reducing NOx emission while simultaneously improving thermal efficiency [8, 9]. Various strategies can achieve LTC in combustion engines. Homogeneous charge compression ignition (HCCI) [10, 11], partially premixed compression ignition (PPCI) [12, 13], and reactivity controlled compression ignition (RCCI) [14]. The strategy that will be researched in this work is RCCI. RCCI has been introduced to overcome the disadvantages of HCCI and PPCI strategies in the direct control of the start of combustion and the combustion rate [15]. It is a dual fuel strategy in which one so-called Low Reactivity Fuel (LRF) and one High Reactivity Fuel (HRF) are used [16]. Utilizing the two fuels, the combustion phase, combustion duration, and magnitude of heat release rate can be controlled [17]. Researchers at the University of Wisconsin-Madison have proven that RCCI combustion can achieve high efficiency and clean combustion [18, 19]. For example, they have shown that RCCI has a better performance in terms of efficiency and emissions at mid-load conditions than conventional combustion [20].

Many researchers have used conventional fuels, gasoline as an LRF and diesel as an HRF, in their studies. E.g., Kokjohn and Benajes used these fuels in their studies [21, 22] to demonstrate the RCCI concept and its advantages. Although fossil fuels are the most convenient and affordable to use as fuel, they are neither renewable nor clean and will deplete in the future [23]. Combining both new advanced LTC strategies with alternative fuel sources has huge potential for cleaner and more efficient combustion. Some examples of alternative LRF possibilities are natural gas [24, 25], syngas [26, 27], alcoholic fuels like methanol [28], ethanol [8], and butanol [15]. Regarding an alternative HRF, biodiesel [29] and dimethyl ether [30] have been investigated. This fuel flexibility of the RCCI strategy is a huge benefit in the optimum design of the engine.

Although RCCI engines with alternative fuels provide significant advantages over other LTC strategies by controlling combustion phasing and maximum pressure rise rates (MPRR), these two factors still limit the RCCI operating range to moderate loads. Ethanol has high resistance to auto-ignition, which provides a large reactivity gradient inside the cylinder to extend the operating range of RCCI engines [31]. In addition, it has a high heat of vaporization and can improve the efficiency and lower NOx emission in RCCI engines [32]. Curran et al. [33] were among the first researchers who investigated the potential benefit of using E85 in a light-duty RCCI engine experimentally. They concluded that replacing gasoline with E85 could significantly extend the high load limit of the engine, and in general, the engine emissions were a little lower with E85. Benajes et al. [34] compared the use of E85 and gasoline as the premixed fuel in a light-duty RCCI engine experimentally and found that E85 can extend the high load limit of the engine by 2 bar at the expense of a little higher emissions. Willems et al. [35] studied the effect of using E85 in a heavy-duty RCCI engine experimentally. They defined a metric to correlate reactivity stratification inside the cylinder to HRR shape and heat loss, and its impacts on combustion efficiency, heat transfer, and NOx emission were explored.

Most of the research done on E85/Diesel engines focuses on experimental work on light duty engines. Achieving higher load operation in heavy-duty engines is more important, and the use of numerical modeling to investigate the effect of the most critical design parameters is missing. It has been shown that CFD modeling can give in depth analysis in the design process of the engine to understand the source of emissions and combustion characteristics by providing 3D visualization of flow parameters which is not possible with experiments. This work aims to numerically investigate the effect of design parameters on all essential parameters including fuel stratification, heat loss, combustion, and emission characteristics in a heavy-duty RCCI engine fueled by E85/diesel with double-step piston geometry.

Effects the start of injection, boost pressure, initial temperature, and spray included angle are investigated. A computational fluid dynamics (CFD) model with detailed kinetic chemistry is built. This CFD model is validated against experimental data obtained by researchers at the Technical University of Eindhoven. The validation is completed by comparing the numerical results of the pressure curve, the heat release rate (HRR), and the engine emissions to that of the experimental data. Following the validation of the CFD model, design parameters will be varied, after which the results are presented and discussed.

2. The computational fluid dynamics model

In this section, the detailed CFD model developed to numerically investigate the effect of design parameters in RCCI engines using E85 as the premixed fuel and diesel as the injected fuel is described. Important topics like CFD software, engine specifications, and numerical models for physical processes, including combustion, spray, turbulence, emissions, and heat transfer, are selected and explained.

2.1 Software description

Please note the following points: In this work the commercially available CFD software CONVERGE is used [36]. CONVERGE is a CFD software for simulating three-dimensional, incompressible, or compressible, chemically-reacting fluid flows in complex geometries with stationary or moving boundaries. CONVERGE features tools such as truly autonomous meshing, adaptive mesh refinement (AMR), fixed embedding, and advanced validated numerical models for physical processes including combustion, spray, turbulence, emissions, and heat transfer. The AMR feature can adapt the generated mesh during runtime, adding cells in areas with large gradients of flow variables to yield more accurate results. At the same time, fixed embedding technology gives the user the ability to define locations within the geometry and time segments to add grid resolution to more accurately resolve critical flow features. Combining AMR and fixed embedding will ensure that the generated mesh is refined when and where it is needed to deal with complex fluid flows.

2.2 Model Description

Experiments were conducted in previous research by Robbert Willems et al. [37] on a single-cylinder of 12.6 liters DAF XEC heavy-duty diesel engine equipped with a common rail system Delphi DFI21 injector and double-step piston at Technical University of Eindhoven. Detailed information of measurements and the experimental setup can be found in [35, 37]. The specifications of this engine are provided in Table 1. The engine rotational speed is maintained at a constant value of 1200 revolutions per minute, and it has a geometrical compression ratio of 15.85, which was lowered from its original value. E85 was injected by a low-pressure injector fitted into the intake port of the cylinder.

Table 1: The specifications of the heavy-duty DAF XEC

Specification	**Value**
Displaced volume	2097 cc
Bore	130 mm
Stroke	158 mm
Connecting rod length	266.7 mm
Piston bowl shape	Double-step
Number of valves	4
Intake valve closure (IVC)	-153 CAD ATDC
Exhaust valve opening (EVO)	128 CAD ATDC
Number of injector holes	7
Hole diameter	0.195 mm
Spray included angle	139°

The IC engine cylinder is axisymmetric. Combining this with the seven equally distributed holes of the high-pressure injector in the middle of the cylinder, the domain can be divided into seven identical portions of 51.4°. The model leverages a structured Cartesian grid with base size of 1.4 mm. Boundary embedding and adaptive mesh refinement were also used to assure the mesh independent solution. A fixed embed scale of one near the piston and cylinder head and a fixed embed scale of two in the vicinity of the injector nozzle, and an AMR embed scale of two for spatial gradients in velocity and temperature. In addition, the fluid flow from IVC to EVO is only simulated, resulting in a further reduction of computational resources needed. This approach reduces the complexity of the complete CFD model because it does not need to include the intake/exhaust valve's motion as they will remain closed. The initial mixture inside the cylinder is considered to be homogeneous. It has been shown that all these simplifications are rational for calculating the essential parameters describing combustion and emissions characteristics concerned in the current study [38]. The result is a simplified CFD model of the DAF XEC heavy-duty diesel engine running RCCI combustion. The visualization of the surface file used can be seen in Fig. 1.

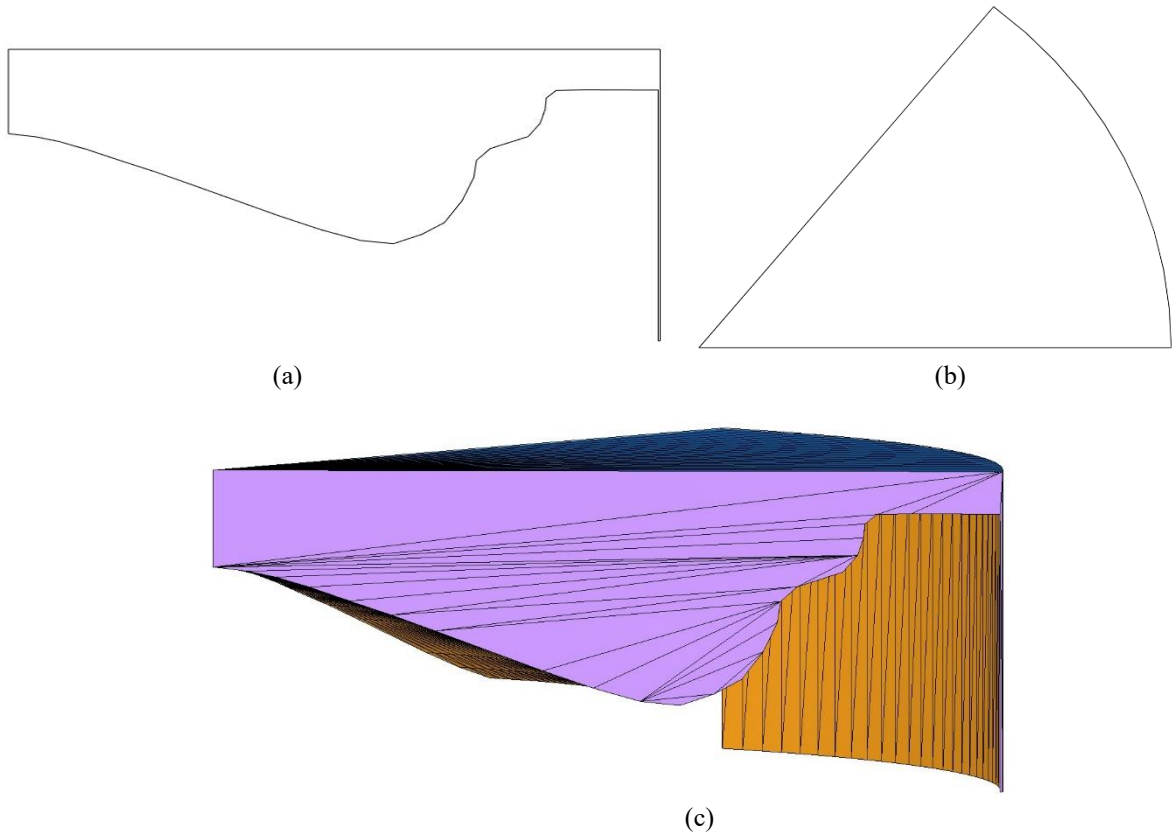

Fig. 1 Planar and upper view sketch of the piston bowl combined with the 3D visualization of the 51.4° surface file of the RCCI engine including the piston crevice region and double-step piston bowl at TDC

2.3 Numerical models

The simulation of the thermophysical and flow processes, including combustion, spray, turbulence, emissions, and heat transfer, requires corresponding models to be selected. There are numerous validated models for these processes implemented in CONVERGE. This section will address the chosen numerical models used in the CFD model. The overview of all the models selected in CONVERGE are presented in Table 2.

Table 2: Overview of the models used in the CFD model using CONVERGE CFD

Phenomenon	Model

Combustion model	SAGE
Combustion chemical kinetics	A reduced PRF-methanol-ethanol-DTBP mechanism [39]
Spray break up	KH-RT
Spray collision model	NTC
Spray wall interaction model	Wall film with O'Rourke splash model
Evaporation model	Frossling
Emission models	Extended Zeldovich NOx model and Hiroyasu-NSC soot model
Turbulence flow	RANS RNG $k-\varepsilon$
Heat transfer model	O'Rourke and Amsden

2.3.1 Combustion model

This work is investigating the combustion of E85 as the LRF and diesel as the HRF. E85 consists of 85% and 15% volume-based percentage of ethanol (C2H5OH) and gasoline, respectively. However, gasoline consists of hundreds of different hydrocarbons. Commonly gasoline is simplified to a single hydrocarbon with somewhat similar thermal and chemical properties, namely isooctane (C8H18), to reduce the computational cost. The lower heating value (LHV) of this blend was set to 29.1 MJ/kg to keep the fuel energy and mass input similar to the experiments of Willems et al. [35, 37]. The result is an LRF blend in the simulation that consists of 69.56 mass-percentage ethanol (C2H5OH) and 30.44 mass-percentage isooctane (C8H18), with the mixture having an LHV of 29.1 MJ/kg. The HRF of diesel consists of hundreds of different hydrocarbon molecules as well. In order to keep the computation cost of the CFD model low, the thermal and chemical properties of n-heptane (C7H16) are used as a substitute for the diesel fuel's properties in the CFD model. N-heptane is frequently used as a substitute for diesel in many numerical studies, and researchers have proven the combustion characteristics are very similar to diesel (e.g., Ra et al. [40]). Similarly, the LHV of n-heptane (C7H16) was set to 42.6 MJ/kg to keep the fuel energy and mass input similar to the experiments data.

CONVERGE provides many options for the non-premixed combustion. This work uses the SAGE model [41] for combustion modeling. SAGE detailed chemistry model uses local conditions to calculate reaction rates based on the principles of chemical kinetics [36]. This solver is fully coupled to the flow solver, but the chemistry and flow solvers parallelize independently, which speeds up the simulation [36]. The SAGE solver requires a chemical kinetic mechanism input file with all the species involved during combustion. The chemical kinetic mechanism consists of thermochemical data for 80 species and chemical rates coefficients for 349 reactions. It has the necessary fuel species which this work requires, i.e., ethanol (C2H5OH), isooctane (C8H18), and n-heptane (C7H16). The reaction mechanism is the reduced PRF-methanol-ethanol-DTBP mechanism developed by Wang et al. [39]. This mechanism has been proposed to simulate the HCCI combustion processes of PRF and alcohol-DTBP fuel mixtures and discover the reactivity enhancement of DTBP to alcohols. It is a frequently used kinetic model in studies with alcohol and isooctane. It has been validated extensively in prediction of IDT and LFS for a wide range of conditions for methanol, ethanol, isooctane, and n-heptane [42].

2.3.2 Spray model

In an RCCI engine, the HRF will be injected directly into the cylinder. This spray of liquid will eventually evaporate and mix with the existing gas mixture inside the cylinder. The spray modeling process introduces fuel droplet parcels into the domain at the specified injector location inside the cylinder. The droplets experiences break up, collision, and evaporation until all fuel droplet parcels are evaporated. For each sub-process, a model has to be selected. The hybrid KH-RT model [43] is commonly used to simulate the DI diesel fuel breakup process. The collision of fuel droplets is modeled using the no time counter (NTC) approach [44]. The Frossling model [45] has been selected to predict the spray evaporation process, and the interaction between the HRF and the wall is done with a wall film model with an O'Rourke splash model [46]. These models were selected based on performance in other studies [47, 48].

As introduced in Section 2.2, the current setup of the CFD model will only simulate a cylinder section. Hence the number of nozzles or injector holes needing to be configured is reduced to 1. The nozzle area is circular with a diameter of 0.195 mm. The nozzle is located in the middle of the cylinder and has the spray included angle of 139°. This angle is defined as an umbrella shape angle of the spray. The injection spray type is a solid cone that starts injecting the fuel at a specified injection rate into the combustion chamber at the SOI. Due to lack of experimental data on the injection rate shape, the default time-dependent profile of Converge CFD software is used.

2.3.3 Emission models

To examine the emissions by the effect of changing design parameters, two extra emission models are implemented in this CFD model. The extended Zeldovich model is used to calculate NO formation [1], and the Hiroyasu-NSC soot model [49] is used to simulate soot oxidation. The model constants are calibrated during the validation stage. CO emission is modeled automatically, since SAGE models detailed kinetic and information on the amount of emitted for these species is available.

2.3.4 Turbulence model

The modeling of turbulence is a critical aspect in predictive and precise combustion simulations. Turbulent motion inside the cylinder is responsible for most of the mixing of fuel and air. It is highly influential on the combustion output parameters and significantly influences the soot emission [50]. The RANS renormalization group (RNG) k-ε turbulence model [50] is chosen in this work. It has been shown in other studies that, the model is not only cost-effective in terms of computational cost but also good enough to predict that most critical engine output parameters [51, 52]. CONVERGE already has set a validated preset for this model, and in this work the values of the default RANS RNG k-ε turbulence model are used.

2.3.5 Heat transfer model

During combustion, the local temperature of up to 2500 Kelvin (K) and the average gas temperature above 1800 K depending on operating conditions are reached. The engine walls are cooled, which induces a temperature gradient between the walls and the charge, generating a heat flux and thus energy losses. These energy losses can be huge, and the heat transfer process must be simulated. Among several validated wall heat transfer models available in CONVERGE, the O'Rourke and Amsden [45] heat transfer model is selected to account for heat transfer through the walls because it is widely used in combustion engine simulation and based on the authors' experience will result in better prediction for the most important combustion characteristics. For simplicity, the piston, liner, and head temperature are set to have the fixed values of 500, 400, and 450 Kelvin, respectively. CONVERGE already has preset values for using this model in IC engines. Fig. 2 depicts a flowchart to show the simulation procedure.

2.3.6 Numerical Solution Procedure

the finite volume method is utilized to discretize the governing transport equation assuring full conservation of flow quantities in the domain. The pressure-velocity coupling is performed using a modified PISO algorithm [53]. The solution algorithm starts with the solution of the momentum equation, which acts as a predictor step. A pressure equation is solved to correct the momentum equation. After the first correction, other transport equations are solved. The procedure is repeated until reaching numerical convergence. In Fig. 2 a flowchart is presented showing all submodels and the numerical solver. More details can be found in the Converge CFD's manual [36].

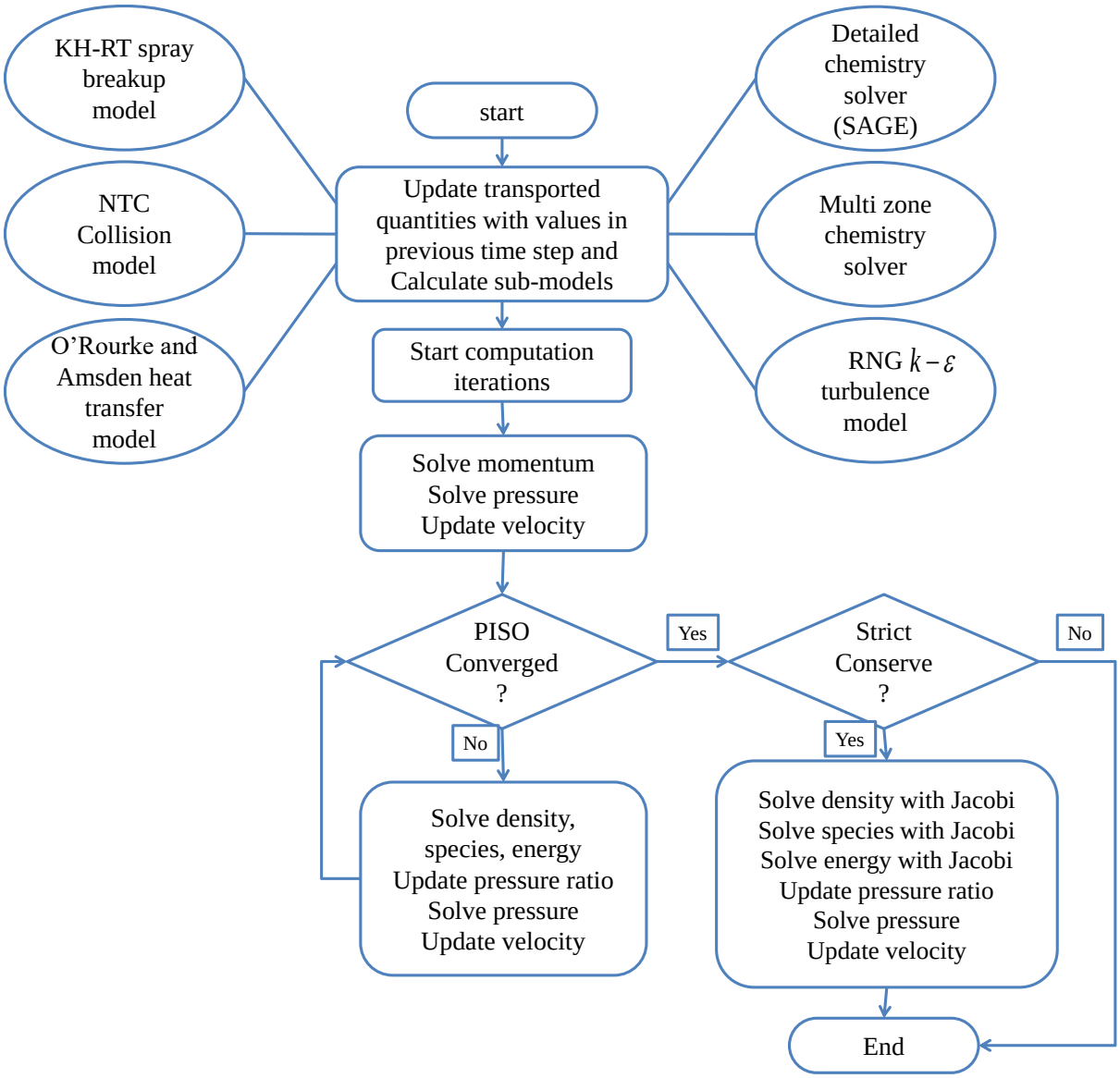

Fig. 2 Flowchart of CONVERGE simulation for a single time step

3. The validation of the CFD model

The CFD model has to be validated against experimental data to trust the results obtained by the numerical CFD model. Experimental data from Willem et al [35, 37] is used to evaluate the CFD model's precision in simulating an RCCI engine. Figure 3 schematically depicts the experimental setup. The complete description of experimental procedure, setup and data collection can be found in the previous research [37]. This section will present the results for combustion, emission, stratification level, and heat transfer characteristics.

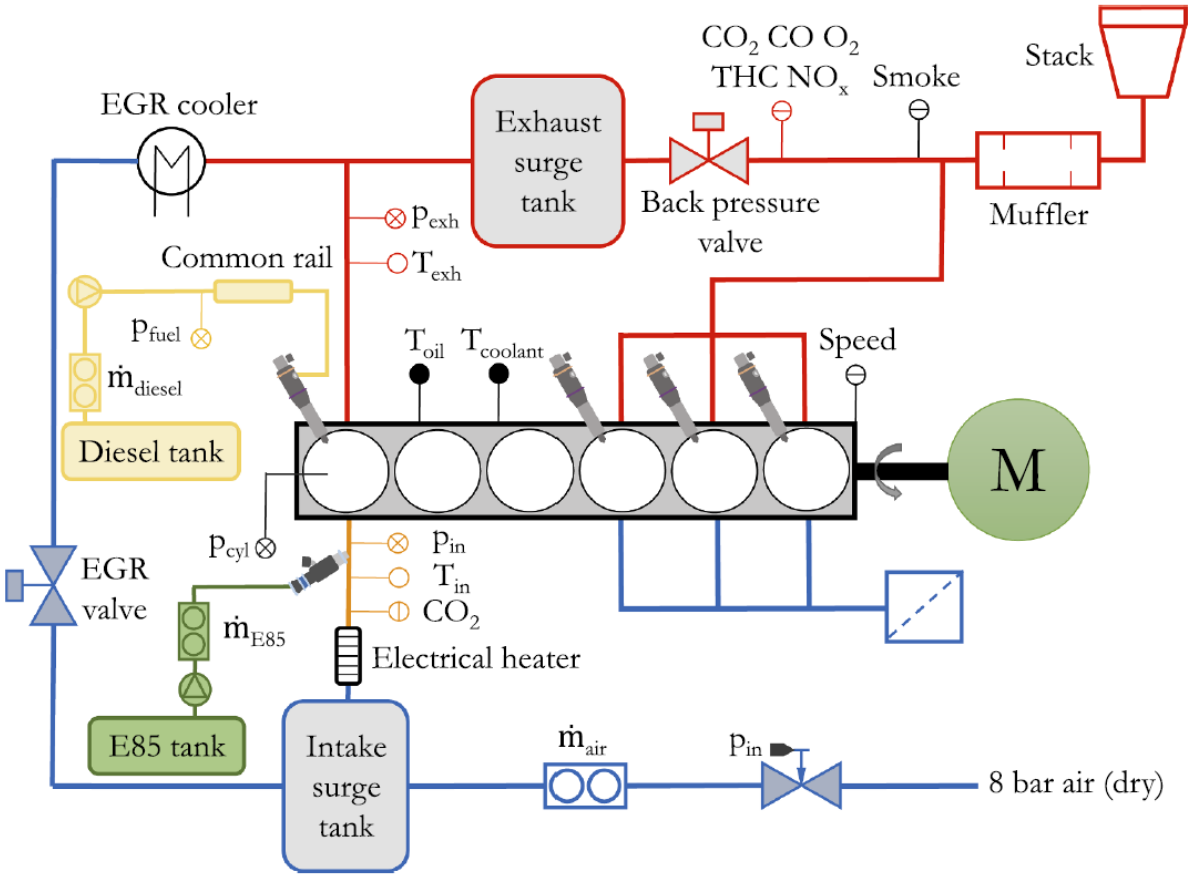

Fig. 3. The schematic diagram of the experimental setup. Blue line shows cold flow and red line shows hot flow.

3.1 The validation process

The validation process of the CFD model is iterative and is based on tuning the parameters which are difficult or impossible to measure during the experiments, and are commonly used in IC engine validation. For example there is no instrument to obtain the actual droplet size distribution of spray. Also, measuring temperature inside the cylinder is very difficult, since the sensor measuring the temperature should be made of special material to tolerate the high temperature during the combustion. According to the study of Senecal [54], the initial temperature at IVC timing should be a little bit higher than the intake temperature. Therefore, in this study, the initial temperature was considered to be higher as well and adjusted accordingly to reach the same combustion timing as we had in the experimental data. Small adjustment were also made the spray model constants which are used to determine the size distribution of droplets inside the domain to match the in-cylinder pressure, the heat release rate behavior, and combustion and emission characteristics, which are fundamental characteristics of IC engines. Only the final result of the validation process will be further discussed in this section.

3.2 The model validation

The experimental data from operating conditions listed in table 3 is selected to validate the CFD model. The operating conditions are chosen to be far away from misfiring and unstable conditions in the engine which have high unburned fuel and pressure rise rate respectively. The EGR value was used to calculate the initial concentration of species at IVC timing. The Combustion Products Calculator tool in Converge was used to calculate the initial mass fractions which leverages the chemical equilibrium solver to compute the initial mass fraction of species at equilibrium.

Table 3: the operating condition of the engine validation case

The engine speed (rpm)	1200
PFI ratio (% by vol)	75.0
SOI ($^{\circ}CA$ ATDC)	-42.5
Intake pressure (bar)	2.0
Intake Temperature (K)	353.0
EGR flow rate (%)	10.0
Air mass flow (g/s)	35.4
Diesel mass flow (g/s)	0.31
PFI fuel mass flow (g/s)	0.9
Common rail pressure (bar)	500

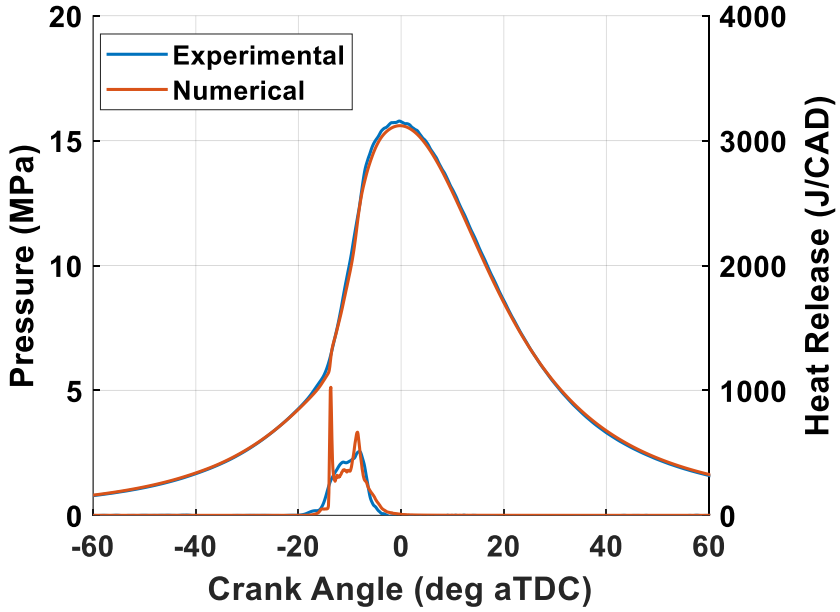

Fig. 4. In-cylinder pressure and heat release rate between -60 and 60 crank angle degrees after top dead center obtained from the experimental data in blue and CFD simulation in orange.

In Figure 4, the results for in-cylinder pressure and HRR of the numerical model and experimental model are presented. As visualized in Figure 4, the CFD model created in CONVERGE accurately predicts the pressure and HRR history of the RCCI engine. The in-cylinder pressure rise rate (the maximum value of the pressure gradient with respect to crank angle) and in-cylinder peak pressure match the experimental data with a maximum deviation of less than 5%. The HRR has a more difference. The HRR curve has a high initial spike because of the chemical mechanism, but it successfully captures dual-stage combustion, usually seen in late injection in RCCI engines [55].

The HRR was further investigated by comparing the combustion phasing and combustion duration. The combustion phasing indicated by the CA50 is in both cases (i.e., the experimental data and numerical simulation) very similar. The combustion duration deviates a bit more but is still within decent margins. To finalize the validation, the emission results are compared and can be seen in Table 4. The soot emissions do not seem to match well, but both values are extremely low and with only an order-of-

magnitude difference. The Hiroyasu soot model is oversimplified since it contains no dependence on the type, composition or structure of the fuel. However it is still sufficient to capture tendencies during the parametric study of the current research. The NOx emission results are different, but they are in the same order of magnitude. The CO emission deviate an order of magnitude from experimental data. And lastly, the CO_2 emissions are relatively good as they are in the same order of magnitude. Although the error between experimental data and simulation results for some of the emissions is high, the exact values for the current parametric study are not so relevant. The simulation values are only used to study how changing design parameters would affect how important output parameters vary.

Table 4: Comparison of CA50, combustion duration, and emissions result from values between the experiments and CFD simulation

	Experiment	**Simulation**	**Absolute Error**
CA50 (deg.ATDC)	-9.96	-9.87	0.0900
Combustion duration (deg)	8.19	7.55	0.6400
Soot emissions (gr/KW.hr)	0.0042	0.222	0.0180
NOx emissions (gr/KW.hr)	10.6	4.085	6.5150
CO emissions (gr/KW.hr)	2.2	0.935	1.2650
CO_2 emissions (gr/KW.hr)	559.1	635.0	75.9000
Efficiency (%)	47.5	44.93	2.57

The validation results indicate that the model developed in this study is able to be predict the in-cylinder pressure, HRR and other combustion characteristics such as combustion duration and phasing accurately. However the model prediction is not very accurate to reproduce the emission values. Nevertheless it is still sufficient to take the emissions trends. Investigating the effects of changing design parameters on the performance of an RCCI engine will be done in the next section. The final verdict of this validated CFD model is that it predicts the current case setup adequately, except for the exact values of the emissions results.

4. Results and discussion

In this section, the CFD results regarding the investigation into the effects of the changing design parameters including the SOI, spray included angle, boost pressure, and initial temperature (IT) on the performance and emissions of an RCCI engine fuelled by E85 and diesel are presented and discussed. The created and validated CFD model is the fundamental starting point for further parametric investigation with only the design parameter altering among simulations.

4.1 Effects of the start of injection

The first design parameter being investigated is the SOI (i.e., the moment this RCCI engine starts its single direct injection strategy). Figure 5 presents the in-cylinder pressure and HRR values between -40 and 40 CAD ATDC for injection timing of -65, -57.5, -50, -42.5, and -35. It is observed that the highest peak pressure occurs in an SOI of -35 CAD ATDC, and this slowly drops in correlation with an advancing SOI to the lowest peak pressure perceived in the SOI of -65 CAD ATDC.

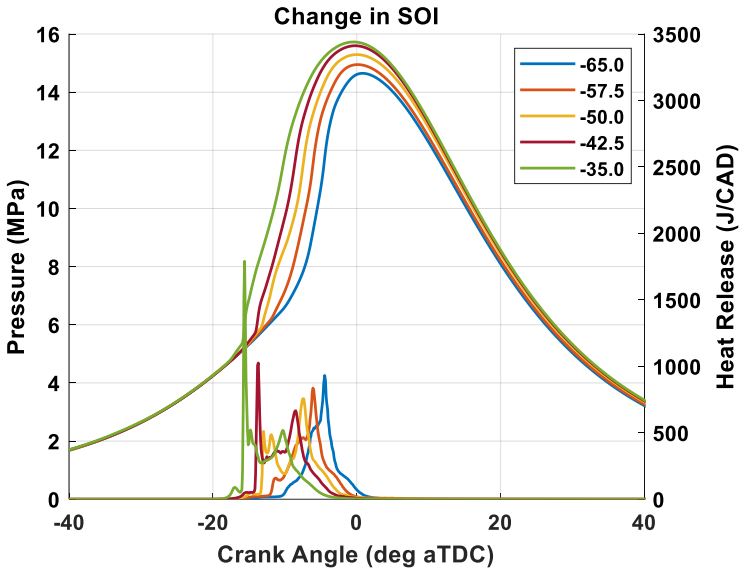

Fig. 5. In-cylinder pressure and heat release rate between -40 and 40 after top dead center obtained from the simulations with -65, -57.5, -50, -42.5, and -35 start of injection (SOI) parameters.

When examining the HRR, the transition towards a single-stage HRR can be seen clearly with the SOI of -65 CAD ATDC having only a single-stage HRR, and the SOI of -35 CAD ATDC having a distinguishable dual-stage HRR. The dual-stage HRR combustion starts in the heavily stratified region, and this region combusts in an intense first part of the combustion, after which the remaining LRF combusts, creating the second stage of the HRR. The single-stage HRR starts in a more centralized location inside the engine cylinder at lower reactivity stratification levels, making the single stage of HRR. The HRR curves also clearly show that the start of ignition retards as the SOI timing advanced away from TDC. Setting forward the SOI allowed the direct-injected diesel more time to distribute, creating a less stratified charge with less concentrated fuel-rich regions resulting in lower local ignitability. The total equivalence ratio inside the engine cylinder is visualized to indicate the level of fuel reactivity stratification. The total equivalence ratio of the E85/diesel dual-fuel engine can be calculated according to Equation 1 derived from the formula in the work of Zheng et al. [56].

$$\varphi = \frac{m_{C_2H_5OH} * 9 + m_{C_8H_{18}} * 15 + m_{C_7H_{16}} * 15.2}{m_{O_2} + m_{N_2}} \quad (1)$$

In the numerator in the equation the mass of each fuel has been multiplied by its stoichiometric AFR (Air-Fuel ratio) value. This equivalence ratio is visualized on cut planes of three simulations at the start of combustion (SOC) presented in Figure 6, where the SOC is defined as the moment where the initial heat release occurs, and the combustion is in the first stage of the dual-stage combustion. The total equivalence ratio distributions on the cut planes of the engine at SOC are vastly different between

the simulations. In the case with SOI of -35 CAD ATDC combustion starts at a high fuel reactivity stratification (the flame location is located at low equivalence ratio, indicating all fuel is burned) as the DI spray is still visible. In comparison, the earlier SOI of -65 CAD ATDC clearly shows a lower level of fuel reactivity stratification.

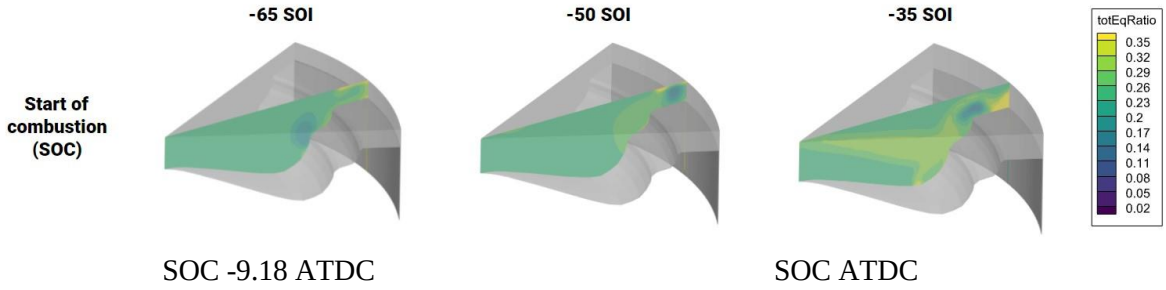

Fig. 6. Total equivalence ratio cut planes at start of combustion (SOC) for -65, -50, and -35 start of injection (SOI) simulations.

This lower level of fuel reactivity stratification produces a shorter single-stage HRR than a high level of fuel reactivity stratification, which creates a longer dual-stage HRR as already stated (see Fig. 5 and 8f). Reducing the fuel reactivity stratification also affects the temperature inside the cylinder considerably as lower equivalence ratio values mixture burns at lower temperatures. This fact can be observed from the contour plot in figure 7, where the local temperature is visualized on the cut planes of three simulations at CA10, CA50, and CA90. As expected, the identified locations with higher equivalence ratio values in Figure 8 result in higher local temperatures. This affect soot and NOx emissions. higher gas temperature increases the NOx emission as NOx formation rates are higher while simultaneously decreasing soot emission since more soot will be decomposed (see Figs. 9b and 9d).

Figure 8 compares six combustion and heat release output parameters of the five different SOI cases. In Figure 8a, the in-cylinder mean gas temperature is visualized. It is observed that by advancing the SOI and decreasing the fuel reactivity stratification, the mean gas temperature drops significantly. In Figure 8b, the heat transfer loss is presented which is calculated by adding up all of the heat transfer values from all boundaries, and the final value is divided by the total input energy that is calculated by the LHV of the fuels. By pulling the SOI away from TDC, the heat transfer loss decreases significantly. This fact correlates with the difference in mean gas temperature, as the advanced SOI simulations create lower in-cylinder temperatures than the delayed SOI simulations.

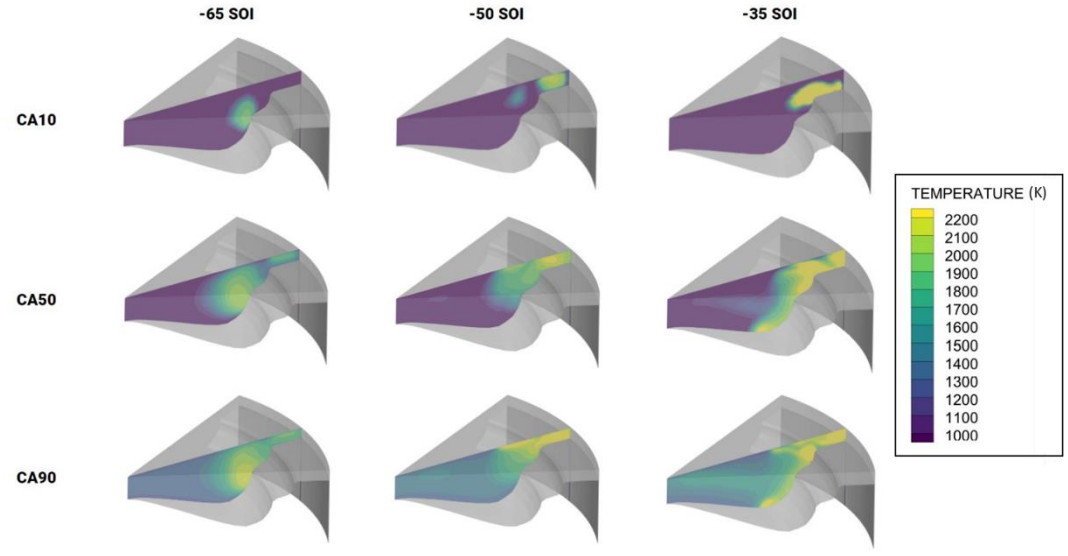

Fig. 7. Temperature cut planes at CA10, CA50, and CA90 for -65, -50, and -35 (ºCA ATDC) start of injection (SOI) simulations.

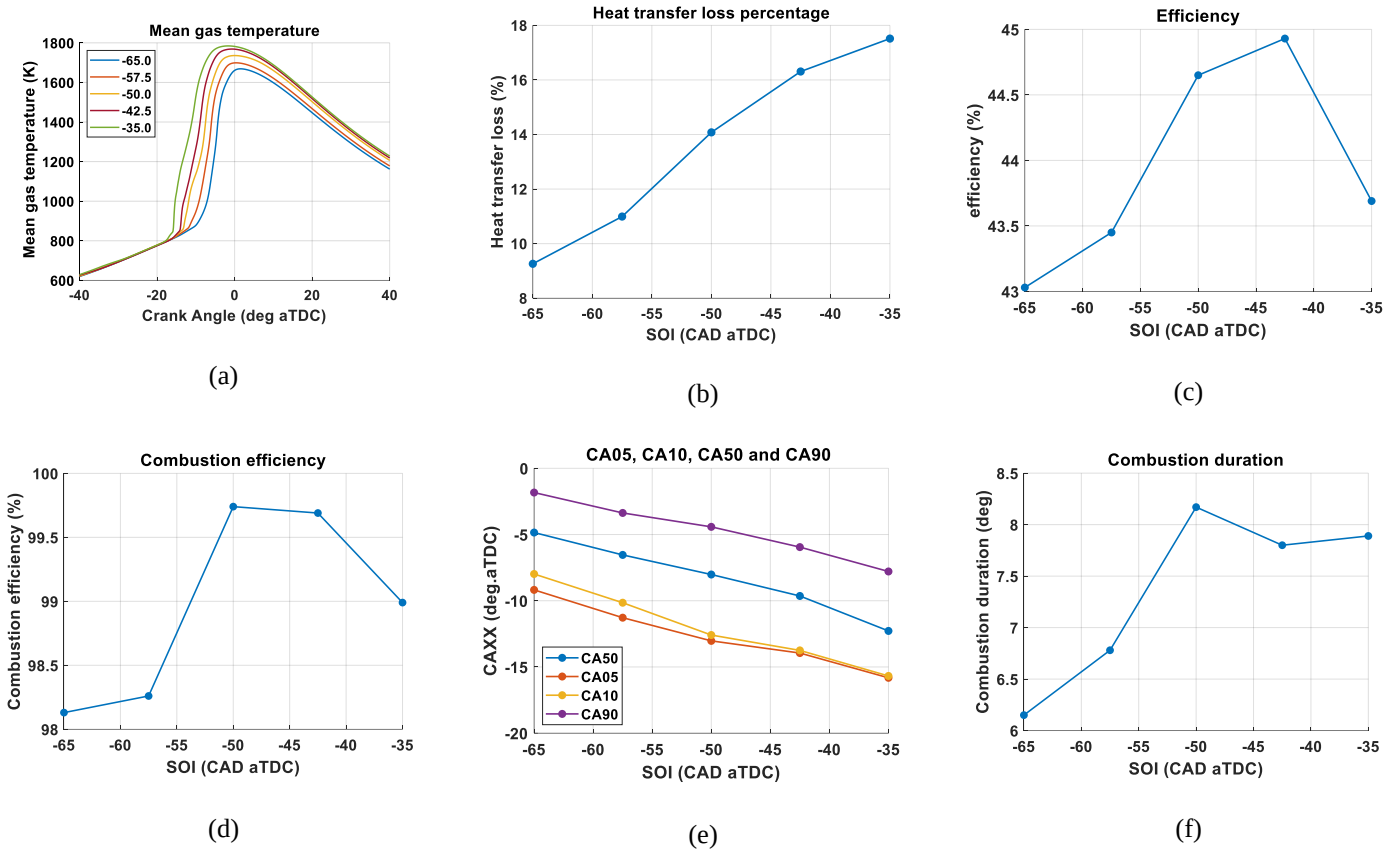

Fig. 8. Combustion and heat release characteristics when varying start of injection timings from -65 to -35 crank angle degrees ATDC with an interval of 7.5 crank angle degrees.

In Figure 8c, the engine's efficiency is presented. The engine efficiency is calculated through dividing the work of the in-cylinder gas mixture by the total input energy of the fuels. The efficiency seems to have an optimum efficiency somewhere in between the cases. This is caused by opposing losses. The gained energy in reducing heat transfer by advancing the SOI gets nullified by the decreased peak pressure due to delayed combustion start, creating less work. While for the case where SOI is -35 CAD ATDC, combustion and consequently the increase in pressure is way too early, and all of the amounts of heat release is during the compression stroke, which causes negative work, thereby significantly reducing thermal efficiency. In Figure 8d, the combustion efficiency is presented. The combustion efficiency is linked to the CO emission results as it represents the total amount of fuel converted to the final product of combustion. The combustion efficiency seems to have an optimum location between the simulations and is impacted by temperature and fuel reactivity stratification. Generally, with higher temperatures, the burning rate of the fuels will be increased, reducing the emissions. But in the case of the too much delayed SOI, the higher local equivalence ratio forms near the cylinder wall (see Fig. 6) causing incomplete combustion.

In figure 8e, crank angles for 5, 10, 50, and 90 percent mass of fuel burned can be seen (i.e., CA05, CA10, CA50, and CA90). The SOC identified with the CA05, CA10, CA50, and CA90 shifts towards TDC when injection happens earlier. Specifically looking at the combustion phasing (indicated by CA50), the trend is observed. The earlier the SOI is, the later the combustion phasing is. Additionally, the less intense first part of the combustion in the earlier SOI simulations is also observed as the offset between CA05 and CA10 increases with an advanced SOI timing. Meanwhile, in the last figure (8f), the combustion duration of the simulations is shown, and it is perceived that by delaying the SOI, the combustion duration increases. This comes from the fact that advancing the SOI produces less fuel reactivity stratification, making the combustion similar to HCCI engines in which the charge auto-ignites suddenly at the same time and closer to TDC.

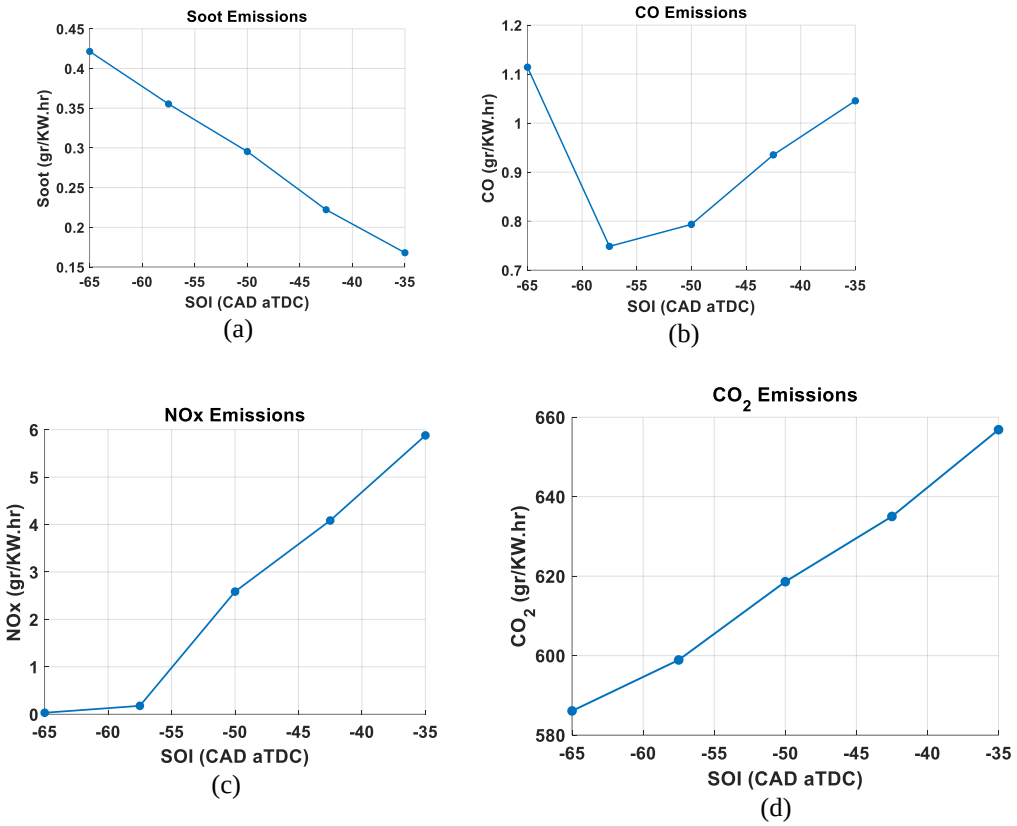

Fig. 9. Variation of emissions results with different start of injection (SOI) timings from -65 to -35 crank angle degree ATDC with an interval of 7.5 crank angle degrees

The final step in the investigation examines the emissions characteristics of the five different simulations. The results in gram per kWh can be seen in Figure 9. The CO emissions seem to have an optimum location where the lowest emissions results are found. It is established that the generated power (which is correlated to the efficiency) mainly determines the shape of the CO emission results. In the CO emission results, two opposing effects are present. Delaying the SOI too much towards TDC leads to more incomplete combustion due to the high fuel stratification (local equivalence ratio). In contrast, advancing the SOI too much results in lower combustion temperatures leading to more incomplete combustion due to too low temperature. The latter only happens in the SOI of -65 CAD ATDC. While CO emission drop and rise with a delayed SOI, the soot, NOx, and CO_2 emissions seem to have only a single response. Setting back the SOI results in the soot emission decrease and NOx and CO_2 emission increase. The soot emission decreases due to the higher combustion temperatures decomposing more soot. Although soot emission is related to the local equivalence ratio as well, it seems the effect of temperature is more prominent. The NOx emission increases with the higher combustion temperatures as NOx formation rates are more noticeable at higher temperatures. The CO_2 emission increases as higher temperatures lead to more complete combustion.

4.2 Effects of boost pressure

The second design parameter being investigated is the boost pressure (i.e., the intake pressure through the inlet manifold). Figure 10 presents the in-cylinder pressure and HRR history from -40 to 40 CAD ATDC for the cases where boost pressures are 1.6, 1.8, 2.0, 2.2, and 2.4 bar. The start of injection and the other operating conditions has been kept the same as table 3. It is observed that the highest peak pressure reached is 17.4 MPa in the simulation of 2.4 bar boost pressure, and this drops to the lowest peak pressure of 13.7 MPa while decreasing boost pressure to 1.6 bar as expected. With increasing pressure the concentration of the molecules in the intake charge elevates and the number of collision between molecules increases subsequently which finally leads the mixture to ignites earlier. Continuing the observations to the HRR, it is perceived that combustion duration in the higher boost pressure is significantly longer. With increasing boost pressure, flame speed decreases due to lower

average temperature. Most notably, the recession of the HRR curve takes longer as the remaining fuel fragments burn out later. This will be even clearer when the crank angles for 90 percent mass of fuel burned (i.e., CA90) are visualized in the second part of this section. Another effect perceived in the HRR is the advanced SOC with the increased boost pressure. The cause can be attributed to an increased mean gas temperature before SOC, causing the charge to reach the necessary ignition conditions earlier. Figure 13a visualized this effect as the mean gas temperature before combustion is indeed different, with the simulations with the higher boost pressure having the highest mean gas temperature before SOC. However, as Figure 11b visualizes, the peak temperature is reduced with increasing boost pressure because of the presence of cooler air [38]. Additionally, the decrease of peak global gas temperature reduces the heat transfer losses (see Fig. 12). Consequently, the NOx emission decreases as a result of the increased boost pressure.

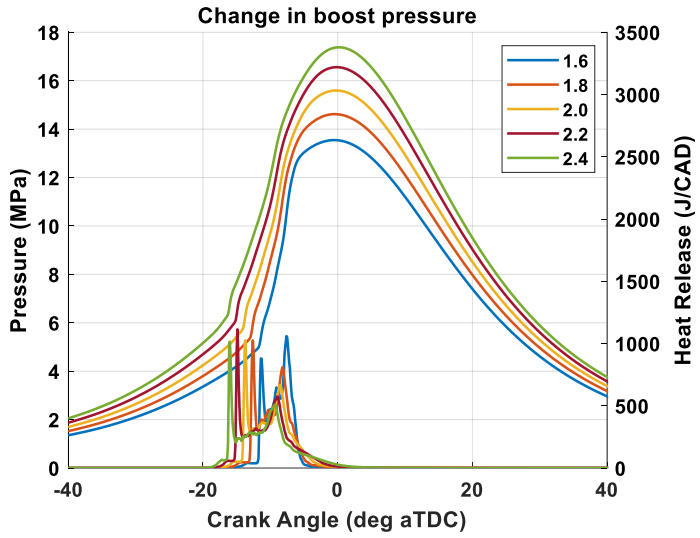

Fig. 10. In-cylinder pressure and heat release rate from -40 to 40 crank angle degrees ATDC obtained from the simulations with boost pressures of 1.6, 1.8, 2.0, 2.2, and 2.4 bar.

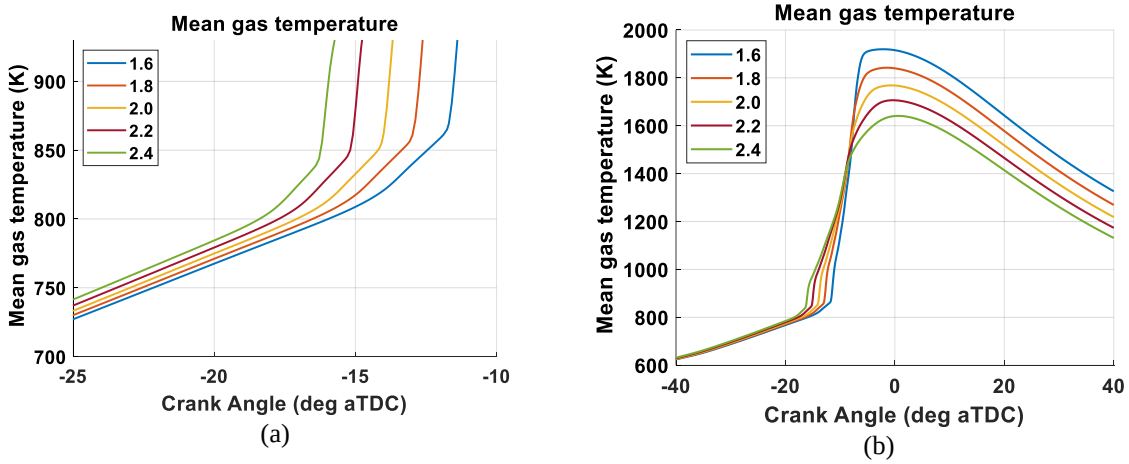

Fig. 11. Mean gas temperature between -25 and -10 (i.e., before SOC) and -40 and 40 crank angle degree ATDC obtained from the simulations with boost pressures of 1.6, 1.8, 2.0, 2.2, and 2.4.

Figure 12 compares five combustion and heat characteristics of the five different boost pressure simulations. In Figure 12a, the percentages of heat transfer loss to the total fuel energy input are presented. The heat loss does not change significantly by altering the boost pressure. Similar finding were also reported in [57] where the effect of boost pressure on heat transfer in an RCCI engine were investigated. Although the average temperature decreases by boosting pressure, as shown in Figure 11b, the heat loss seems to be influenced by combustion duration, maximum local temperature, and flame distance from the walls as well. The outputs of the model shows that increasing intake pressure raises the maximum local temperature slightly. In Figure 12b, the engine's efficiency is presented. The engine efficiency is the ratio of the useful work done to the heat provided by combustion. As visualized in the figure, the efficiency seems to have an optimum efficiency somewhere between the simulations. The

efficiency is affected by the amount of energy loss, combustion phasing, and peak pressure. In general, higher peak pressure and less heat loss contribute to improved efficiency; however, combustion phasing should not be too early, which produces negative work during the engine's compression stroke. In this case, the gained energy in increasing peak pressure by boosting intake pressure gets nullified by the advanced start of combustion, creating less work. The combustion and consequently the increase in pressure is way too early, and all of the heat released is not used to produce work, thereby reducing thermal efficiency.

In Figure 12c, the combustion efficiency is presented. The combustion efficiency is linked to the CO emission results as it represents the total amount of fuel converted to the final product of combustion. As perceived in the figure, the combustion efficiency decreases with increasing boost pressure. In Figure 12d, crank angles where 5, 10, 50, and 90 percent of fuel mass burned can be seen. It shows that CA05, CA10, CA50, and CA90 shift away from TDC with higher boost pressures. The higher the boost pressure is, the earlier the combustion phasing is. Additionally, the increased burning duration is noticeable, with the CA90 moving closer to TDC with increased boost pressure. And in the last Figure 12e, the combustion duration of the simulations is shown. By increasing the boost pressure, the combustion duration increases significantly.

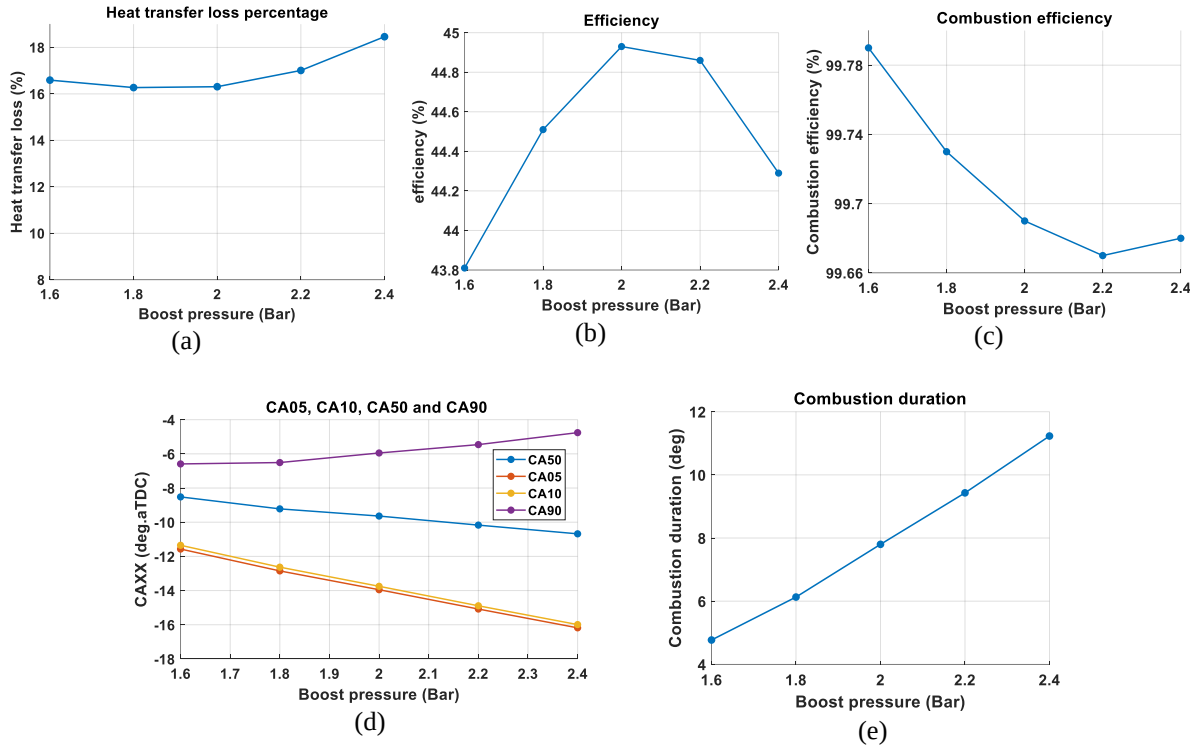

Fig. 12. Combustion and heat release characteristics with varying boost pressures between 1.6 and 2.4 bar with an interval of 0.2 bar.

The emission characteristics are presented in gram per kWh in Figure 13. Similar to the engine response with change in SOI, both the CO and CO_2 emissions seem to have an optimum location at which the lowest emission results are found. The CO emission results are determined, and two opposing effects are presented as an explanation. It is observed that increasing the boost pressure too much seemed to result in lower combustion temperatures leading to incomplete combustion. It also increase the amount of oxygen in the mixture and CO conversion to CO_2 is facilitated. This is seen in the highest boosted case. In contrast, decreasing the boost pressure leads to faster combustion because of the higher average temperature. Thus increasing the boost pressure reduces the CO emission, as long as the temperature is not too low.

While the CO, and CO_2 emissions drop and rise with increased boost pressure, the soot and NOx emissions seem to have monotonic behavior. The soot emissions are linked to the in-cylinder local equivalence ratio and temperature. in-cylinder local equivalence ratio is almost identical in all cases since the premixed equivalence ratio, injection timing, and amount of injected diesel fuel are the same. But the temperature decreases with increasing boost pressure, resulting in increased soot emissions

due to less oxidation. The NOx emission results are heavily linked to the in-cylinder temperature, which decreases with increasing boost pressure, resulting in reduced NOx emission.

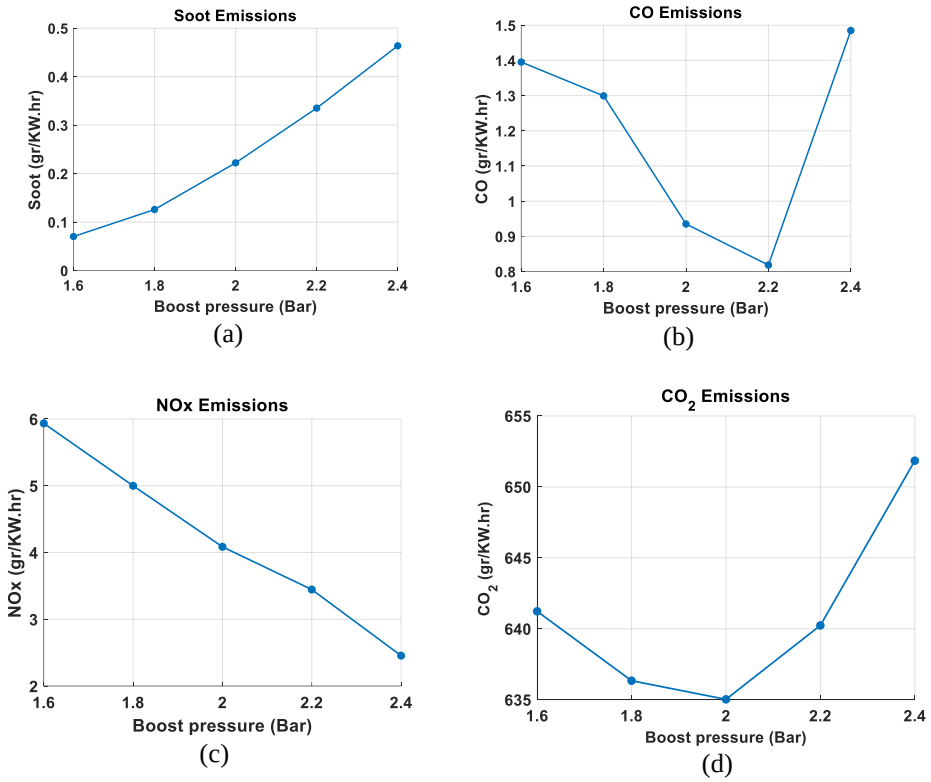

Fig. 13. Emissions results with varying boost pressures between 1.6 and 2.4 bar with an interval of 0.2 bar.

4.3 Effects of initial temperature

The initial temperature (i.e., the temperature of the premixed charge at the start of IVC) is another critical parameter that mainly affects the mixture's burning rate. Figure 14 demonstrates the in-cylinder pressure and HRR values between -40 and 40 CAD ATDC for different initial temperatures of 313, 333, 353, 373, and 393 kelvin. The start of injection and the other operating conditions has been kept the same as table 3. It is seen that the highest peak pressure reached is 15.6 MPa in the simulation, where the initial temperature is 353 kelvin. Generally higher initial temperature has two important effects. Firstly, It leads to more complete, faster combustion, and accordingly higher peak pressure due to less unburned fuel. However, it also alters the combustion phasing and the amount of air mass. Too advanced combustion timing results in more negative work and lower peak pressure. Thus peak pressure first elevates and then reduces. Regarding HRR, it is perceived that combustion duration in the higher initial temperature simulations is significantly shorter. Most notably, the shape of the HRR seems the same but compressed with a more intense HRR. The reason for this compressed and more intense HRR is that with an increased temperature, the necessary activation energy for the chemical reaction to occur is achieved easier, consequently increasing the reaction rates resulting in a quicker HRR. Another effect perceived in the HRR is the advanced SOC with raising the initial temperature. The observed cause is the increased mean gas temperature before SOC, causing the charge to reach the necessary temperature conditions for ignition earlier. Still the efficiency increasing with reducing the initial temperature because of the reduced heat loss (fig. 15b) and improved combustion phasing fig (15c).

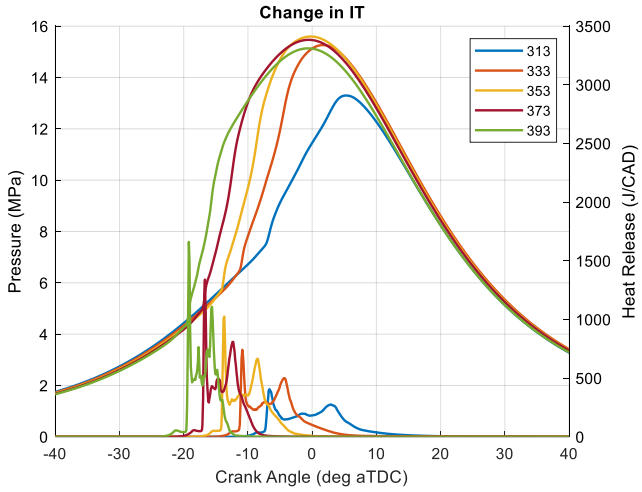

Fig. 14. In-cylinder pressure and heat release rate between -40 and 40 crank angle degree after top dead center obtained from the simulations with 313, 333, 353, 373, and 393 Kelvin initial temperature (IT)

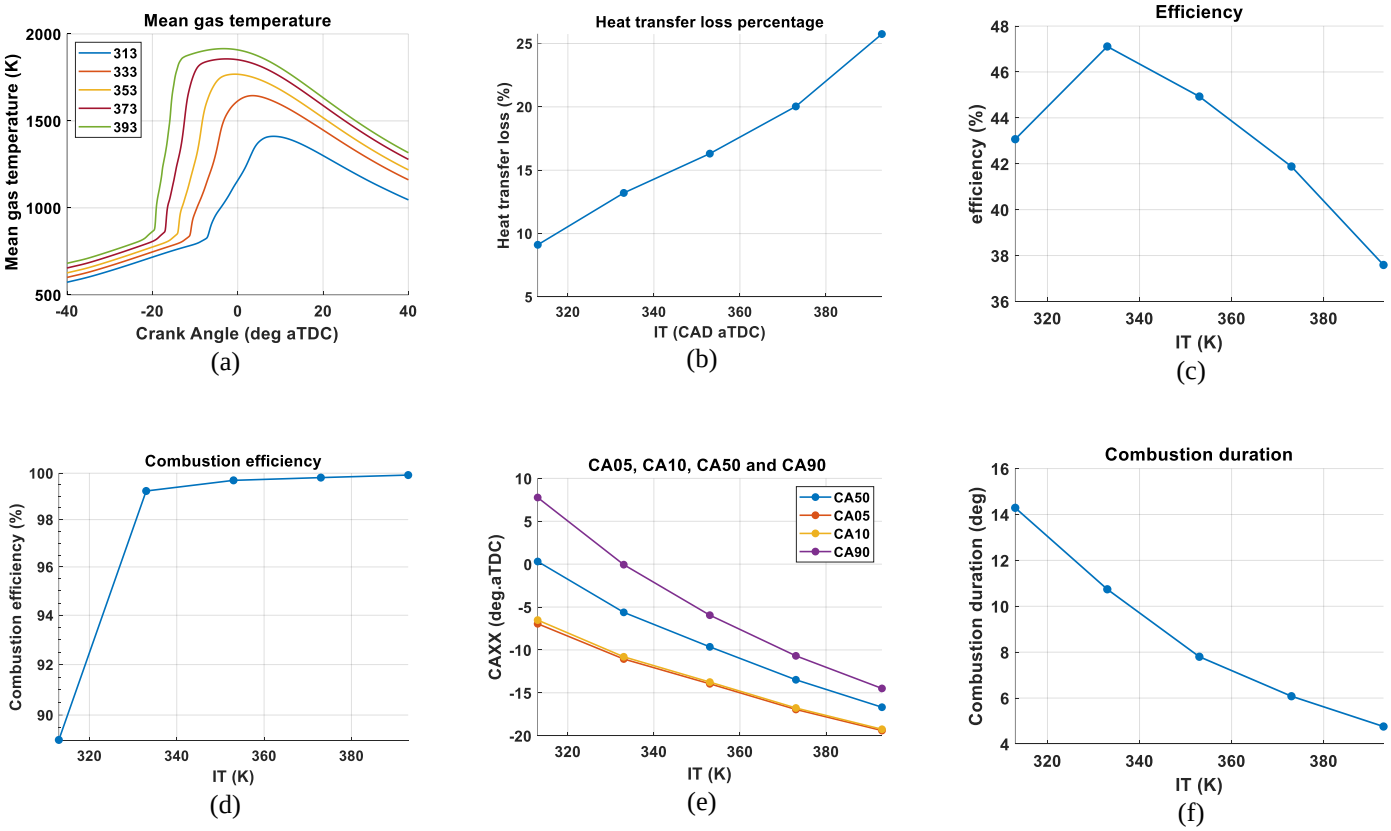

Fig. 15. Combustion and heat release characteristics with varying initial temperatures between 313 and 393 Kelvin with an interval of 20 Kelvin.

The global mean gas temperature of the charge is significantly higher with elevated initial temperatures (see Fig. 15a). Consequently, this would affect the heat transfer loss percentage as higher heat fluxes are present, as visible in Figure 15b. In Figure 15c, the engine's efficiency is presented. When the initial charge is too hot, the efficiency is decreased, for the gain in combustion efficiency is less than the energy percentage lost by heat transfer. Additionally, the work provided by the higher initial temperature is too early, consequently further reducing the thermal efficiency. Figure 15d visualizes the combustion efficiency. It is seen that the change in combustion efficiency rapidly increases by

decreasing initial temperature. This is, of course, caused by the increased incomplete combustion occurring at lower temperatures. In Figure 15e, the crank angles where 5, 10, 50, and 90 percent of fuel (by mass) is burned can be seen. With increasing initial temperature, SOC is advanced by going away from TDC, and the offset between CA10, CA50, and CA90 is reduced with more intense HRR. And lastly, Figure 15f visualized the decreased combustion duration, already discussed in the previous section.

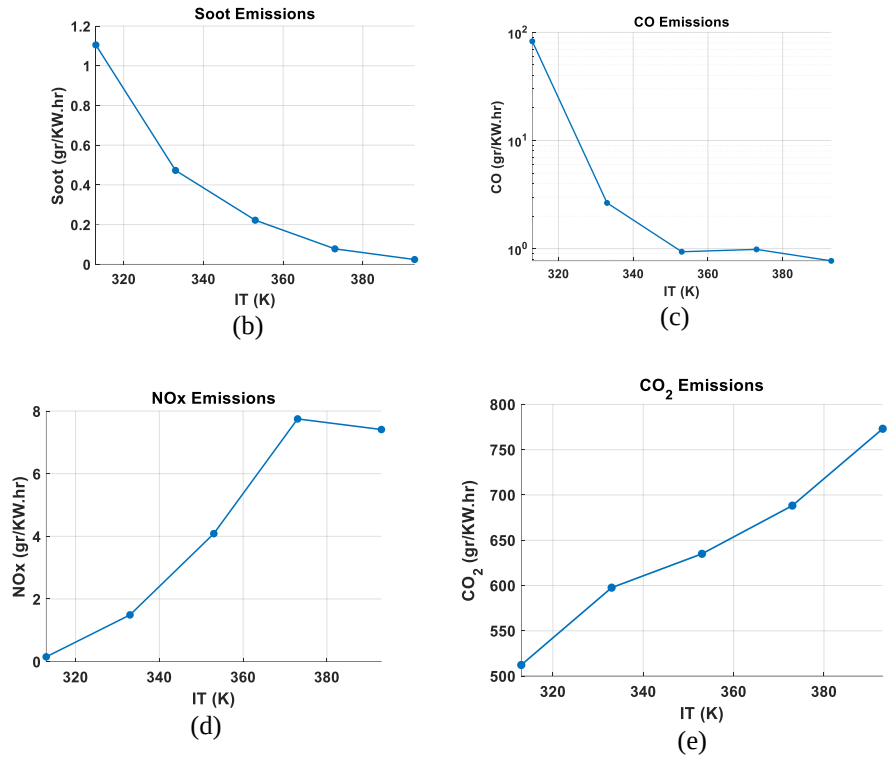

Fig. 16. Emissions results with varying initial temperatures between 313 and 393 kelvin with an interval of 20 kelvin.

The effect on emission characteristics is presented in Figure 16. As expected, soot, and CO emissions decrease with increasing initial temperature. The CO emission decrease because combustion will be more complete at higher temperatures. At higher temperature the amount of air mass also decrease. However, faster burning rate outweighs the effect of the air mass. The soot emissions decrease as the higher temperatures result in more soot being oxidized before EVO. The NOx emission is higher at higher initial temperatures as the increased temperature results in higher in-cylinder gas temperature resulting in higher NO formation rates.

4.4 Effects of spray included angle (Umbrella angle)

Umbrella angle (UA) in RCCI engines can determine where the combustion starts inside the engine's cylinder. Figure 17 represents the contour of the total equivalence ratio in cut planes for different Injection Angles (IAs) which are defined here to be the half of UA. In the case of the injection angle of 40 degrees, the geometry of the piston directs diesel fuel from the center of the cylinder to the bowl's double step location, and the fuel moves toward the liner. When the angle is 50 degrees, the spray more or less hits the lower step head-on. This keeps the fuel mostly inside the bowl and combustion occurs at the same location. But when the angle is 60 degrees, the fuel hits the edge of the lower step, and its path branches into two, which causes the flame to initialize in two different parts. Finally, in the case of the injection angle of 70 degrees, the fuel hits the wall of the cylinder and accumulates mostly above the piston squeeze area. The flame is initialized and moves from the liner into the bowl. Note that for this case, the flame starts near the cylinder wall and the crevice region, it burns all the fuel trapped in that area, and because these areas are the source of HC emission, it causes HC emissions to decrease.

Normally smaller injection angles cause the flame to start closer to the central axis inside the cylinder, and it does not reach the area near the crevice region, and as shown in the figure, some fuel remains unburned near the cylinder wall and crevice region.

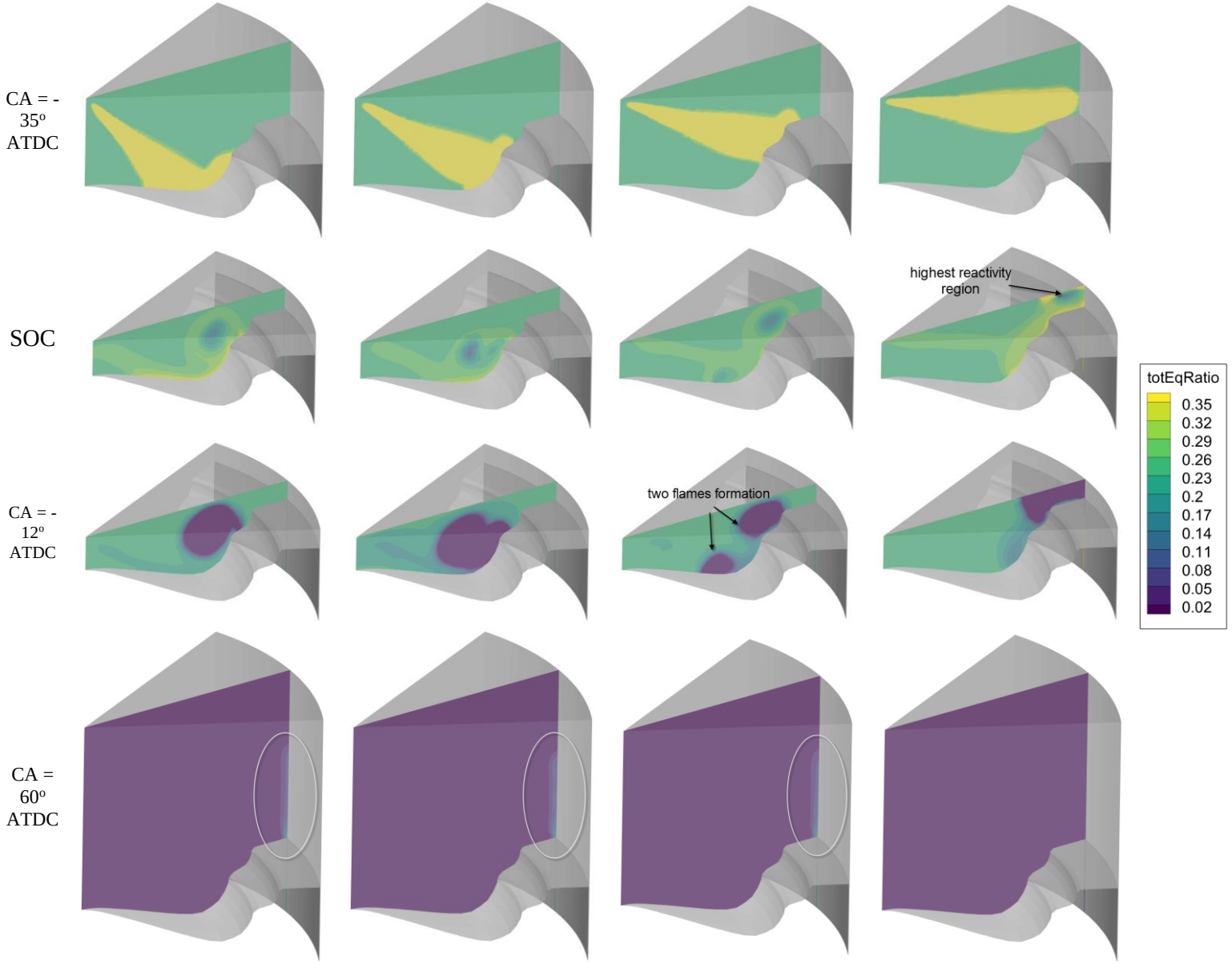

Fig. 17. Total equivalence ratio cut planes at -35 deg. ATDC, start of combustion (SOC), -12 deg. ATDC, and 60 deg. ATDC for different injection angles.

Figure 18 shows the in-cylinder pressure and HRR values for the different injection angles. The start of injection and the other operating conditions has been kept the same as table 3. As we can see, there is no significant difference among the results. The peak pressure in the case of injection angle of 69.5 degrees is a bit higher than other cases because there is less unburned fuel discussed in the contour plot of equivalence ratio. As a result, the combustion and thermal efficiency are improved with larger injection angles (See Figs. 19c, 19d). The HRR curves for the injection angles of 69.5 and 50 have a higher initial spike. The reason behind the initial spike can be attributed to the fact that in these two cases, the amount of fuel accumulation in one location is higher than in the other cases (as we discussed in the previous section). In the other two cases, fuel tends to mix better, resulting in less fuel accumulation in one place. One further important observation from the HRR curves is that the latest rise of the HRR curve corresponds to the case with the highest injection angle. This can be attributed to hitting fuel to the cylinder liner, which has a lower temperature than the piston crown resulting higher heat loss since the fuel hits the piston crown in all of the other cases. It can also be observed the case

with largest IA has two peaks. This can be due to the burning of the fuel trapped in the crevice region later on during the combustion process.

Figure 19 depicts the important output parameters. The average temperature inside the cylinder is a bit higher for the largest injection angle because of more complete combustion. The heat loss is also higher with a larger injection angle, considering that the flame is formed near the cylinder liner where the highest heat transfer occurs. Since the combustion phasing in all the cases is almost the same, thermal efficiency will be determined mainly by combustion efficiency and heat loss. The combustion efficiency is higher for the largest injection angle because of less incomplete combustion, and it seems its effect outweighs the heat loss on the thermal efficiency. Combustion phasing and duration do not change significantly, which was also found from HRR curves. However, there is a slight difference in the combustion duration results.

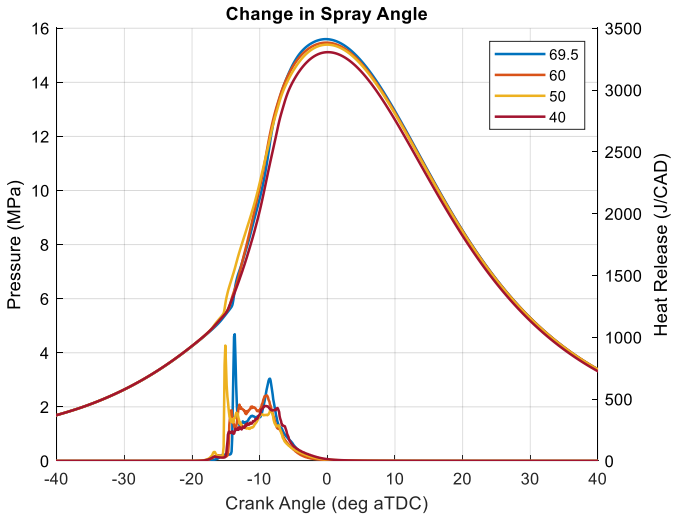

Fig. 18. In-cylinder pressure and heat release rate between -40 and 40 crank angle degree after top dead center obtained from the simulations with different injection angles

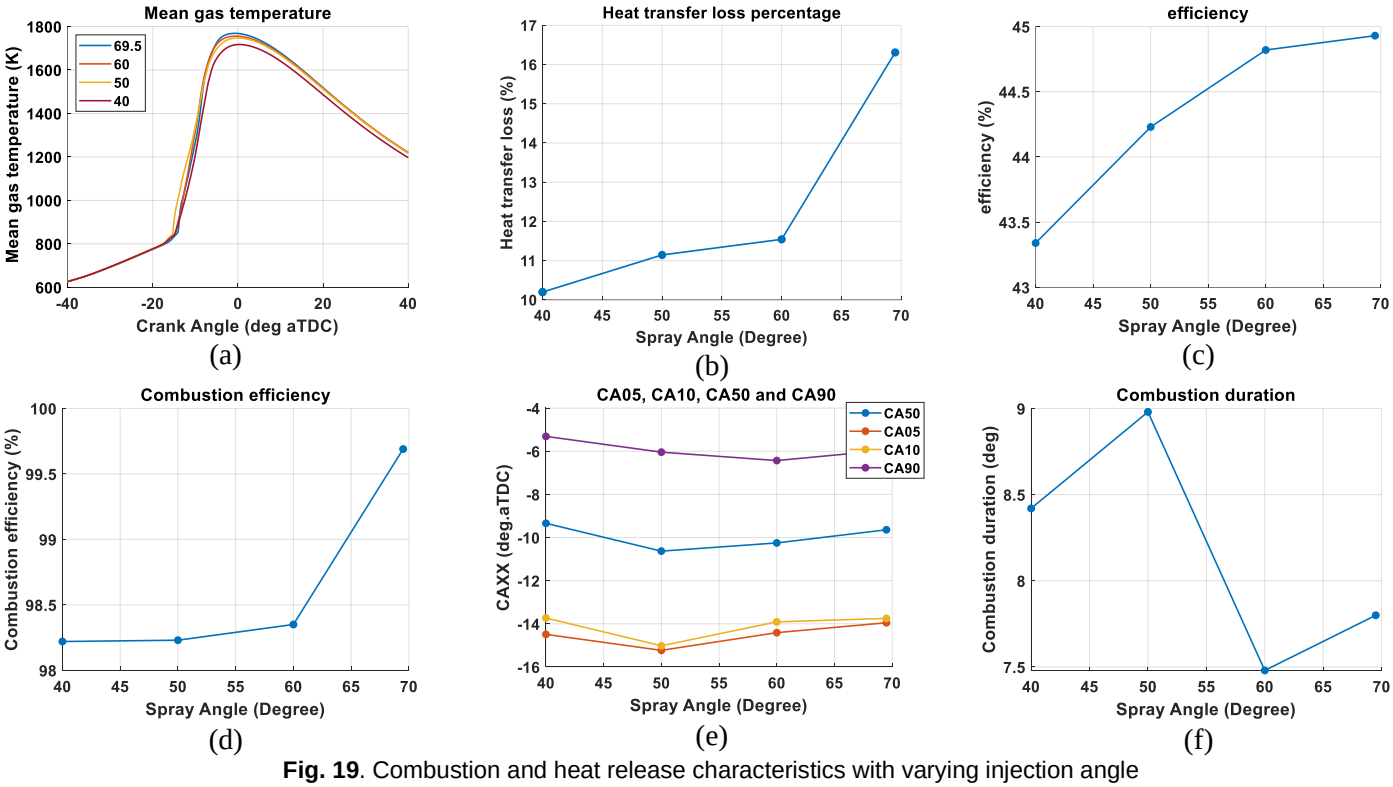

Fig. 19. Combustion and heat release characteristics with varying injection angle

The results of engine emissions can be perceived in Figure 20. As expected, the soot, and CO emissions decrease with injection angles because of more complete combustion and a bit higher temperature at higher injection angles. The soot emissions decrease marginally as the average temperature is a bit higher at larger angles, while the maximum local equivalence ratios are the same in all cases. As a consequence of fixed combustion phasing and the lower emission results of CO and soot, CO_2 emission increase because of the more complete combustion. Regarding the NOx emission, since the average temperature is almost the same among the cases, it is mainly determined by combustion duration and start of combustion. The combustion duration is most prolonged when the injection angle is 50 degrees resulting in higher NOx emission since NOx formation is slow process and when the charge is given more time NOx emission will be higher.

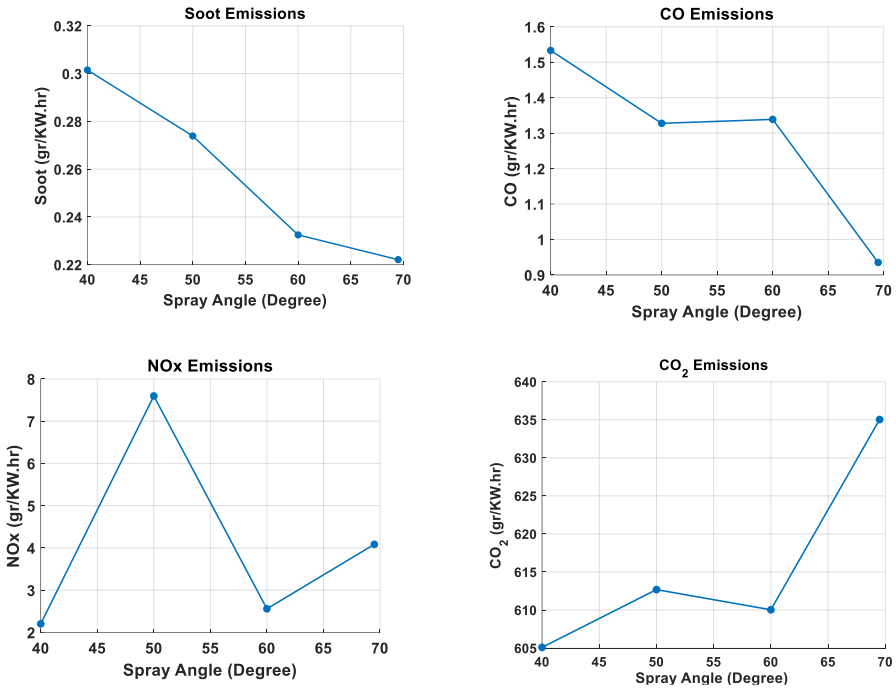

Fig. 20. Emissions results with varying injection angle

Conclusions

This work performed a parametric investigation on the effects of the SOI, boost pressure, initial temperature, and spray included angle in a heavy-duty RCCI engine fuelled by E85/diesel with double step piston bowl geometry. Their impacts on the stratification level, heat transfer, performance, and emission characteristics were studied. In the research on the effect of changing SOI, it became clear that fuel reactivity stratification, local equivalence ratio, and the shape of the HRR curve are influenced by a change in SOI. It was found that by keeping the stratification levels low with an early SOI, the total heat loss inside the combustion chamber can be reduced. However, the fuel reactivity stratification level should not become too low, as combustion efficiency and thermal efficiency will decrease. This concludes that the optimum timing corresponds to a moderate stratification level (in this work caused by an SOI around -46 CAD ATDC).

In the investigation into the effect of boost pressure, it became clear the boost pressure primarily influenced the global gas temperature, combustion duration, HRR shape. With higher boost pressure, the recession of the HRR curve takes longer as the remaining fuel fragments burn out later. Also, the mean gas temperature before SOC increased, causing the charge to ignite earlier. Nevertheless, peak average temperature reduced significantly with higher boost pressure. Besides, It was found that heat transfer losses does not change significantly with boost pressure, and it is more related to maximum local temperature (flame temperature) rather that maximum average temperature. Although increasing the boost pressure would, in most cases, considerably reduce NOx, and CO emissions by providing higher oxygen levels, the boost pressure cannot be increased indefinitely, as thermal and combustion efficiency decreases, not to mention the engine's lifetime because of elevated max pressure inside the cylinder.

Moreover, it became clear that the initial temperature massively impacts the global gas temperature. It was found that by decreasing the initial temperature, the overall global gas temperature was reduced. With the reduced overall gas temperature, heat transfer losses can be mitigated. The initial temperature is preferred to be as low as possible but sufficiently high enough to burn all the introduced fuel and keep most of the combustion period before TDC. Otherwise, thermal efficiency will decrease again. It was found that keeping the temperature low is at the cost of higher CO, and soot emissions. Finally, it realized that the injection angle (IA) and piston bowl geometry could substantially affect the flame formation location. Two flames could be formed at the same time by changing IA. The HRR shape, emission, and performance characteristics of the engine were influenced by IA as well. Preferably the flame should form near the cylinder liner and cylinder head rather than the piston bowl to reduce HC emission and increase combustion efficiency. Flame formation near the wall means higher heat loss. Additionally, IA could not alter the combustion phasing, but it could change fuel stratification inside the cylinder, and combustion duration is also affected. It was also found that the initial spike in HRR shape stems from fuel accumulation in one location inside the cylinder.

References

[1] Heywood JB. Internal combustion engine fundamentals: McGraw-Hill Education; 2018.
[2] Kakaee A-H, Rahnama P, Paykani A, Mashadi B. Combining artificial neural network and multi-objective optimization to reduce a heavy-duty diesel engine emissions and fuel consumption. Journal of Central South University. 2015;22:4235-45.
[3] Reitz RD, Ogawa H, Payri R, Fansler T, Kokjohn S, Moriyoshi Y, et al. IJER editorial: the future of the internal combustion engine. SAGE Publications Sage UK: London, England; 2020.
[4] Novella R, Bracho G, Gomez-Soriano J, Fernandes CS, Lucchini T. Combustion system optimization for the integration of e-fuels (Oxymethylene Ether) in compression ignition engines. Fuel. 2021;305:121580.
[5] Novella R, Gomez-Soriano J, Martinez-Hernandiz PJ, Libert C, Rampanarivo F. Improving the performance of the passive pre-chamber ignition concept for spark-ignition engines fueled with natural gas. Fuel. 2021;290:119971.
[6] Pan S, Cai K, Cai M, Du C, Li X, Han W, et al. Experimental study on the cyclic variations of ethanol/diesel reactivity controlled compression ignition (RCCI) combustion in a heavy-duty diesel engine. Energy. 2021;237:121614.
[7] Krishnamoorthi M, Malayalamurthi R, He Z, Kandasamy S. A review on low temperature combustion engines: Performance, combustion and emission characteristics. Renewable and Sustainable Energy Reviews. 2019;116:109404.
[8] Han J, Somers LMT, Cracknell R, Joedicke A, Wardle R, Mohan VRR. Experimental investigation of ethanol/diesel dual-fuel combustion in a heavy-duty diesel engine. Fuel. 2020;275:117867.
[9] Kakaee AH, Rahnama P, Paykani A. Numerical study of reactivity controlled compression ignition (RCCI) combustion in a heavy-duty diesel engine using 3D-CFD coupled with chemical kinetics. Automotive Science and Engineering. 2014;4:792-804.
[10] An Y, Jaasim M, Raman V, Pérez FEH, Sim J, Chang J, et al. Homogeneous charge compression ignition (HCCI) and partially premixed combustion (PPC) in compression ignition engine with low octane gasoline. Energy. 2018;158:181-91.
[11] Schröder D, Banke K, Kaiser SA, Atakan B. The kinetics of methane ignition in fuel-rich HCCI engines: DME replacement by ozone. Proceedings of the Combustion Institute. 2021;38:5567-74.
[12] Tanov S. Investigation of Partially Premixed Combustion in an Optical Engine: In-Cylinder Flow and Combustion Characterization. Ph.D. Thesis: Lund University; 2017.
[13] Zhang Y, Cho K, Sellnau M. Investigation on Combining Partially Premixed Compression Ignition and Diffusion Combustion for Gasoline Compression Ignition—Part 2: Compression Ratio and Piston Bowl Geometry Effects. SAE International Journal of Sustainable Transportation, Energy, Environment, & Policy. 2021;2.
[14] Kokjohn SL. Reactivity controlled compression ignition (RCCI) combustion. 2012.
[15] Han J, Somers B. Effects of Butanol Isomers on the Combustion and Emission Characteristics of a Heavy-Duty Engine in RCCI Mode. SAE Technical Paper; 2020.
[16] Paykani A, Garcia A, Shahbakhti M, Rahnama P, Reitz RD. Reactivity controlled compression ignition engine: Pathways towards commercial viability. Applied Energy. 2021;282:116174.

[17] Benajes J, García A, Monsalve-Serrano J, Sari RL. Experimental investigation on the efficiency of a diesel oxidation catalyst in a medium-duty multi-cylinder RCCI engine. Energy Conversion and Management. 2018;176:1-10.
[18] Splitter D, Hanson R, Kokjohn S, Reitz RD. Reactivity controlled compression ignition (RCCI) heavy-duty engine operation at mid-and high-loads with conventional and alternative fuels. SAE Technical Paper; 2011.
[19] Hanson R, Kokjohn S, Splitter D, Reitz R. Fuel effects on reactivity controlled compression ignition (RCCI) combustion at low load. SAE International Journal of Engines. 2011;4:394-411.
[20] Kavuri C, Kokjohn SL. Computational optimization of a reactivity controlled compression ignition (RCCI) combustion system considering performance at multiple modes simultaneously. Fuel. 2017;207:702-18.
[21] Benajes J, Molina S, García A, Belarte E, Vanvolsem M. An investigation on RCCI combustion in a heavy duty diesel engine using in-cylinder blending of diesel and gasoline fuels. Applied Thermal Engineering. 2014;63:66-76.
[22] Kokjohn SL, Hanson RM, Splitter DA, Reitz RD. Fuel reactivity controlled compression ignition (RCCI): a pathway to controlled high-efficiency clean combustion. International Journal of Engine Research. 2011;12:209-26.
[23] Han J. Alcohol applications in heavy-duty diesel engines. Ph.D. Thesis: Technische Universiteit Eindhoven; 2020.
[24] Bekdemir C, Baert R, Willems F, Somers B. Towards Control-Oriented Modeling of Natural Gas-Diesel RCCI Combustion. SAE Technical Papers. 2015;2015-April.
[25] Rahnama P, Paykani A, Reitz RD. A numerical study of the effects of using hydrogen, reformer gas and nitrogen on combustion, emissions and load limits of a heavy duty natural gas/diesel RCCI engine. Applied energy. 2017;193:182-98.
[26] Chuahy FDF, Kokjohn SL. Effects of reformed fuel composition in "single" fuel reactivity controlled compression ignition combustion. Applied energy. 2017;208:1-11.
[27] Rahnama P, Paykani A, Bordbar V, Reitz RD. A numerical study of the effects of reformer gas composition on the combustion and emission characteristics of a natural gas/diesel RCCI engine enriched with reformer gas. Fuel. 2017;209:742-53.
[28] Li Y, Jia M, Xu L, Bai X-S. Multiple-objective optimization of methanol/diesel dual-fuel engine at low loads: A comparison of reactivity controlled compression ignition (RCCI) and direct dual fuel stratification (DDFS) strategies. Fuel. 2020;262:116673.
[29] Hanson RM, Reitz RD. Effects of biofuel blends on transient reactivity-controlled compression ignition engine combustion. International Journal of Engine Research. 2016;17:857-65.
[30] Park SH, Shin D, Park J. Effect of ethanol fraction on the combustion and emission characteristics of a dimethyl ether-ethanol dual-fuel reactivity controlled compression ignition engine. Applied Energy. 2016;182:243-52.
[31] Dempsey AB, Walker NR, Reitz R. Effect of cetane improvers on gasoline, ethanol, and methanol reactivity and the implications for RCCI combustion. SAE International Journal of Fuels and Lubricants. 2013;6:170-87.
[32] Dempsey AB, Das Adhikary B, Viswanathan S, Reitz RD. Reactivity Controlled Compression Ignition Using Premixed Hydrated Ethanol and Direct Injection Diesel. Journal of Engineering for Gas Turbines and Power. 2012;134.
[33] Curran S, Hanson R, Wagner R. Effect of E85 on RCCI Performance and Emissions on a Multi-Cylinder Light-Duty Diesel Engine. SAE International; 2012.
[34] Benajes J, García A, Monsalve-Serrano J, Villalta D. Benefits of E85 versus gasoline as low reactivity fuel for an automotive diesel engine operating in reactivity controlled compression ignition combustion mode. Energy Conversion and Management. 2018;159:85-95.
[35] Willems R, Willems F, Deen N, Somers B. Heat release rate shaping for optimal gross indicated efficiency in a heavy-duty RCCI engine fueled with E85 and diesel. Fuel. 2021;288:119656.
[36] Richards KJ, Senecal, P.K., and Pomraning, E.,. CONVERGE 3.0, Convergent Science. Wisconsin Madison, 2021.
[37] Willems RC. Designed experiments for efficient engines. Ph.D. Thesis: Technical University of Eindhoven; 2020.
[38] Rahnama P, Arab M, Reitz RD. A Time-Saving Methodology for Optimizing a Compression Ignition Engine to Reduce Fuel Consumption through Machine Learning. SAE International Journal of Engines. 2020;13:267-88.
[39] Wang H, Dempsey AB, Yao M, Jia M, Reitz RD. Kinetic and Numerical Study on the Effects of Di-tert-butyl Peroxide Additive on the Reactivity of Methanol and Ethanol. Energy & Fuels. 2014;28:5480-8.

[40] Ra Y, Yun JE, Reitz RD. Numerical parametric study of diesel engine operation with gasoline. Combustion Science and Technology. 2009;181:350-78.
[41] Senecal PK, Richards KJ, Pomraning E, Yang T, Dai MZ, McDavid RM, et al. A new parallel cut-cell Cartesian CFD code for rapid grid generation applied to in-cylinder diesel engine simulations. SAE Technical Paper; 2007.
[42] Rahnama P, Bao H, Somers B, Paykani A, Novella R. A chemical kinetic study of low alcohol/iso-octane blends in both premixed and partially premixed combustion. 2021.
[43] Beale JC, Reitz RD. Modeling spray atomization with the Kelvin-Helmholtz/Rayleigh-Taylor hybrid model. Atomization and sprays. 1999;9.
[44] Schmidt DP, Rutland CJ. A new droplet collision algorithm. Journal of Computational Physics. 2000;164:62-80.
[45] Amsden AA, O'Rourke PJ, Butler TD. KIVA-II: A computer program for chemically reactive flows with sprays. Los Alamos National Lab.(LANL), Los Alamos, NM (United States); 1989.
[46] O'Rourke PJ, Amsden AA. A spray/wall interaction submodel for the KIVA-3 wall film model. SAE transactions. 2000:281-98.
[47] Meng X, Meng S, Cui J, Zhou Y, Long W, Bi M. Throttling effect study in the CDF/RCCI combustion with CNG ignited by diesel and diesel/biofuel blends. Fuel. 2020;279:118454.
[48] Hao C, Lu Z, Feng Y, Bai H, Wen M, Wang T. Optimization of fuel/air mixing and combustion process in a heavy-duty diesel engine using fuel split device. Applied Thermal Engineering. 2021;186:116458.
[49] Hiroyasu H, Kadota T. Models for Combustion and Formation of Nitric Oxide and Soot in Direct Injection Diesel Engines. SAE Transactions. 1976;85:513-26.
[50] Han Z, Reitz RD. Turbulence modeling of internal combustion engines using RNG κ-ε models. Combustion science and technology. 1995;106:267-95.
[51] Sener R, Yangaz MU, Gul MZ. Effects of injection strategy and combustion chamber modification on a single-cylinder diesel engine. Fuel. 2020;266:117122.
[52] Kumar A. A CFD study on DME/Methanol fuelled unconventional RCCI. M.Sc. Thesis: Technical University of Eindhoven; 2021.
[53] Issa RI. Solution of the implicitly discretised fluid flow equations by operator-splitting. Journal of computational physics. 1986;62:40-65.
[54] Senecal PK. Development of a methodology for internal combustion engine design using multi-dimensional modeling with validation through experiments: The University of Wisconsin-Madison; 2000.
[55] Guerry ES, Raihan MS, Srinivasan KK, Krishnan SR, Sohail A. Injection timing effects on partially premixed diesel–methane dual fuel low temperature combustion. Applied Energy. 2016;162:99-113.
[56] Zheng J, Wang J, Zhao Z, Wang D, Huang Z. Effect of equivalence ratio on combustion and emissions of a dual-fuel natural gas engine ignited with diesel. Applied Thermal Engineering. 2019;146:738-51.
[57] Hendricks TL, Splitter DA, Ghandhi JB. Experimental investigation of piston heat transfer under conventional diesel and reactivity-controlled compression ignition combustion regimes. International Journal of Engine Research. 2014;15:684-705.